



Assumption
University

Digital Commons @ Assumption University

Honors Theses

Honors Program

2020

Self-Organization of Cosmic Elements During Stellar Evolution

Travis Butler
Assumption College

Follow this and additional works at: <https://digitalcommons.assumption.edu/honorsthesis>



Part of the [Physics Commons](#)

Recommended Citation

Butler, Travis, "Self-Organization of Cosmic Elements During Stellar Evolution" (2020). *Honors Theses*. 57.
<https://digitalcommons.assumption.edu/honorsthesis/57>

This Honors Thesis is brought to you for free and open access by the Honors Program at Digital Commons @ Assumption University. It has been accepted for inclusion in Honors Theses by an authorized administrator of Digital Commons @ Assumption University. For more information, please contact digitalcommons@assumption.edu.

Self-Organization of Cosmic Elements During Stellar Evolution

Travis Butler

Faculty Supervisor: Georgi Georgiev, Ph.D.

Department of Biological and Physical Sciences

A Thesis Submitted to Fulfill the Requirements of the
Honors Program at Assumption College

Fall 2019

Contents

1 Introduction	1
1.1 Quantity-Quality Transition	4
2 Methods	4
2.1 Varying Explosion Energies	5
3 Theory	6
3.1 Model	6
4 Results	6
5 Discussion	9
6 Conclusion	10
Acknowledgement	11
References	11

Self-Organization of Cosmic Elements During Stellar Evolution

Travis Butler

Faculty Supervisor: Georgi Georgiev

Department of Biological and Physical Sciences, Assumption College

A Thesis Submitted to Fulfill the Requirements of the Honors Program at Assumption College

An open question in science is how complex systems self-organize to produce emergent structures and properties. One aspect is to find the dependence of structure and organization on the size of a system. It has long been known that there is a quality-quantity relationship in natural systems, which is to say that the properties of system depend on its size. More recently, this has been termed the Size-Complexity Rule. In this Thesis paper, we study the average rates of nucleosynthesis and action efficiency of stars with varying initial metallicities and explosion energies from simulations (Nomoto, Tominaga, Umeda, Kobayashi, & Maeda, 2006) based on the Stellar Abundances for Galactic Archaeology database (Suda et al., 2008). Our goal is to study the size-complexity relation in stars of varying metallicities and explosion energies and to compare them with other complex systems. Here, as a measure of complexity of a star, we are using the grouping and approximate number of reactions of nucleons into heavier elements, because they increase the variety of elements and changes the structure of the star. Then we calculate the average rate of grouping of nucleons by multiplying each of them by their level of grouping, defined as how many of them are joined into a nucleus, and then divide by the lifetime of the star over which these isotopes were synthesized. As seen in our previous work, complexity, as measured by action efficiency grows exponentially in time and as a power law of all other characteristics of a system, including its size. Here we find that, as for the other systems studied, the complexity of a star in terms of grouping of its elements and the rate of increase of complexity is a power law of its size despite differing explosion energies and initial metallicities. As shown by these stars, the bigger a system is, the higher the levels of complexity it can reach even if the initial metallicity and explosion energy are different. This is seen in how each star's progress, average rate, flow, and action efficiency of nucleosynthesis dramatically increase as a function of their initial number of nucleons. Our goal is to find how universal the size-complexity relation is, and whether there are any exceptions. We are planning to study other systems to find whether they obey the same rule and, as stellar evolution simulations improve, to study in detail not just the average rate, but the instantaneous rate of nucleosynthesis.

1 Introduction

The Big Bang produces all the matter present in the universe in the form of mostly Hydrogen and trace amounts of Helium. Lithium was negligible compared to Hydrogen and Helium. Eventually, large amounts of hydrogen atoms coalesced and created their own gravity, which forced these atoms together in a dense space. This forces many of the hydrogen atoms together, which released energy and heat. The heat force opposes the force of gravity and has continued to form new elements through nucleosynthesis. Stellar nucleosynthesis begins after the gravitational collapse of a dense, molecular cloud into a protostar. The mass of the protostar determines if it will reach the temperatures necessary for nuclear fusion and become a star. Towards the end of a star's life, however, it inefficiently forms heavier elements beyond iron, which absorbs heat and energy instead of releasing them. Eventually, the star no longer has as much

of the force of heat to oppose gravity, which collapses in on itself and explodes (Thielemann, Diehl, Heger, Hirschi, & Liebendörfer, 2018). Therefore, the complex systems that are being examined in this Thesis paper are stars and their action of synthesizing elements throughout the course of their lifetime until they explode in a supernova event. When stars go supernova, they release the elements that were made over the course of their life. This includes the heavier elements, like iron, that would not be visible before the supernova. The elemental abundances can then be detected using spectrometry instruments to determine the amount of each element produced.¹

¹ β_n is the total number of nucleons from each isotope within the star. β_i is the initial total number of nucleons present in each star. M_\odot is the solar mass of the Sun in kilograms. M_{is} is the mass of the isotope present in the star in solar masses. M_{cut} is the total mass of metals compact at the center of the star throughout its lifetime. N_A

The data represents the nucleosynthesis yields as a function of initial metallicity and stellar mass from nucleosynthesis yields of core collapse supernovae and galactic chemical evolution. It was used to prove that the progress of nucleosynthesis and average rate of nucleosynthesis obeys a power law as a function of size, as shown in the previous papers. These yields are based on the new developments in the observational and theoretical studies of supernovae and extremely metal-poor stars in the halo, which have provided excellent opportunities to test the explosion models and their nucleosynthesis (Nomoto et al., 2006). In this Thesis paper, the initial metallicities of the stars studied are 0.000, 0.001, 0.004, and 0.02. Their masses range from 13 to 40 solar masses when only the metallicity varies. Additionally, we also study when these stars have varying explosion energies. The masses for these range from 13 to 40 solar masses with a metallicity range from 0.000 to 0.02.

The goal of this research is to show and confirm the power law behavior of the progress, average rates, flow, and action efficiency of nucleosynthesis as a function of the initial number of nucleons in spite of varying metallicities and explosion energies. This is to compare to our model (Georgiev et al., 2015) and make a conclusion if stars behave in the same way as other complex systems, which is the size-complexity or quantity-quality relation. This is to say that the complexity, measured by the number of nucleons combined into heavier nuclei, is a function of the star's size. We also study the rate of complexity increase in addition to the level of complexity itself. This compares to our previous papers on CPU evolution: Level of organization and quantity were found to be in a positive feedback, and to increase exponentially in time, and as a power law of each other. Our research aims to show a similar trend with stars undergoing nucleosynthesis. Much research about stellar systems has been devoted to collecting the elemental abundances of stars from nearby galaxies. Several reports (Umeda & Nomoto, 2003) (Frebel et al., 2005) have talked about how abundances in HE0107-5240 and other extremely metal poor stars are in good accord with nucleosynthesis that happens in 20 to 130 solar mass stars. Elemental abundances for smaller stars, red giants, were reported in Omega Centauri (Johnson & Pilachowski, 2010). Other research (Wanajo, Nomoto, Janka, Kitaura, & Müller, 2009) has studied the yield and nucleosynthesis of unstable elements and reported their abundance for ST and FP3 model stars. Further simulations (Tominaga, Iwamoto, & Nomoto, 2014) present Pop III SN models whose nucleosynthesis yields individually reproduce the abundance patterns of 48 metal-poor stars. Observations of abundances found in extremely poor-metal stars, HE 1300+0157, have also been done (Frebel et al., 2007). Another study (Prantzos, Abia, Limongi, Chieffi, & Cristallo, 2018) shows how abundance evolution of elements from Hydrogen to Uranium occur in the Milky Way halo through a chemical evolution model of

metallicity dependent isotopic yields from large stars. Some chemical abundances of extremely metal-poor stars from Pop III stars have been shown to describe the nature of first generation stars formed after the Big Bang (Nomoto, Tominaga, Umeda, & Kobayashi, 2005) (Steigman, 2007). Abundance information is critical to our research because, based the stellar information (Nomoto et al., 2006), based on known abundances (Suda et al., 2008), we have determined the abundances of elements that have been created by nucleosynthesis at the end of the star's life. Seeing other researchers search for the abundances of stars and simulated stars shows that it is possible to apply our findings to theirs and see how efficient nucleosynthesis is in both massive and small-scaled stars.

Other stellar research has been done on stars to see how their nucleosynthesis and supernova event describes the chemical evolution of our galaxy using observational data of supernovae and metal-poor stars (Nomoto, Kobayashi, & Tominaga, 2013). Similar research has been done on how these yields (Nomoto et al., 2006) (Nomoto et al., 1997) (Nomoto et al., 2013) are affected by hydrodynamic effects during hypernova and supernova explosions (Nomoto & Suzuki, 2013). Other research has been done on nucleosynthesis to accurately understand the abundance pattern of Pop III stars leading to hypernovae (Nomoto, 2016). Nucleosynthesis yields have also been used to distinguish high-density Chandrasekhar-mass models and lower-density white dwarfs (Mori et al., 2018). These are important because they show that patterns about chemical evolution and nucleosynthesis have been found in past work (Nomoto et al., 2013) (Nomoto, 2016). Later simulations have looked at and utilized the heavy-flavor neutrinos emitted from proton stars, like SN1987A, for triggered parameter explosions (Sinha et al., 2017) (Curtis et al., 2018) to more accurately report chemical evolution and iron group nucleosynthesis yields of in proto-neutron stars, taking into consideration the electron fraction of the ejecta. Another simulation has been done to look at the stellar yields of the first supernovae

is Avagadro's number. ψ is the combined solar masses of Helium-3 and Helium-4. M_* is the mass of the star in solar masses. $140\text{-}\chi$ represents the approximate mean isotope of the periodic elements more advanced than Gallium. $100\text{-}\rho$ is the approximate mean isotope for the elements that were made by a previous star in the metallicity of this paper's stars. ϵ_i is the progress of nucleosynthesis for a selected individual isotope. A is the mass number of a selected isotope. ϵ_{sum} is the total progress of nucleosynthesis within each star before normalization. P is the normalized progress of nucleosynthesis. τ is the lifetime of the star in 10^{10} years. η is the average rate of nucleosynthesis over the course of the star's life. ϕ is the flow of the star, which is the number of nucleon combinations to make each isotope. σ_{iso} is the number of atoms formed from grouping nucleons into isotopes. α is the action efficiency of stars. h is the Plank's constant. L is the luminosity. E_L is the energy emitted from the luminosity. E is the energy absorbed to nucleosynthesis elements. k is the energy fraction from the luminosity.

in stars of 12 to 140 solar masses and how rotation affects the nucleosynthesis yields (Takahashi, Umeda, & Yoshida, 2014). Simulations on nucleosynthetic yield for asymptotic giant branch, white dwarf, and core collapsing stars have been performed (Ritter et al., 2018) (Pignatari et al., 2016). We find that the model of Nomoto 2006 is the best for studying average rates of nucleosynthesis as suggested by other reports (Wanajo et al., 2009), because it shows the abundances of isotopes of various metallicities and solar massed stars. More recent studies of nucleosynthesis have not shown the chemical abundances of isotopes when initial metallicities and explosion energies vary. These results are useful in comparing the ability of various sized stars at various initial metallicities and explosion energies to determine whether various stars follow the Size-Complexity Rules (Bonner, 2004). Many of the recent papers above have discussed abundance levels in different simulated stars, however, none of them have reported their star's yields as thoroughly as Nomoto.

In this Thesis paper, we study how the size of stars affects their ability to form and organize new elements from hydrogen. Earlier research by (Hall, Johnson, & Haas, 1967) has suggested that size has minimal impact on structure and organization in their findings about bureaucratic organizations. Despite the size of the company, (Hall et al., 1967) showed that there was not enough variation in spatial dispersion, hierarchical differentiation, and divisions of labor between large and small bureaucracies. However, later research has shown that the Size-Complexity Rule is valid, as evident in cells that form spherical structures (Amado, Batista, & Campos, 2018) (Bell & Mooers, 1997). Research has been conducted (Bonner, 2015) (Bonner, 1995) to study size-complexity in genetics and the biological life cycle.

Further, the interdisciplinary nature of the Size-Complexity Rule was suggested (Bonner, 1993) (Bonner, 2004) when these papers described how the diversity of occupations increased as population increased in states of India. Several other researchers have also cited Bonner in expanding the Size-Complexity Rule to fit their field of study (Cockburn, Crabtree, Kobti, Kohler, & Bocinsky, 2013) (Holbrook, Barden, & Fewell, 2011).

Biological studies will often use the term "quality-quantity rule" when talking about how an organism's size is directly related to the number of its varying subdivisions, such as its cells. Regardless, these studies are still using the Size-Complexity Rule that J.T Bonner talks about in (Bonner, 2004). Research has been done in biology to show that the Size-Complexity Rule is applicable to different kinds of species (Rosenzweig et al., 1995). Size increase leading to complexity increase has been seen evolutionarily in viruses, single celled prokaryotes, single celled eukaryote and non-colonial multicellular eukaryotes, suggesting that biological complexity increases as the size of the organism increases

(Heim et al., 2017). Biological complexity has been traced on the path from microbes in the early anoxic atmosphere to the biological larger complexity of the contemporary aerobic biosphere microbes (Finlay & Esteban, 2009). Other research has shown that as the number of cells present in amoebas, ciliates, seaweed, green algae, and plants increases, the diversity of cells in those organisms also increased. This trend has also been seen in the measurement of biodiversity in invaded and un-invaded woodlands as the rarefied species richness increases as the number of plants increases (McGlenn et al., 2019). A similar trend in earthworms across North America is seen as the number of earthworms increases, the species diversity increases (Gaston, 2000). The same is true for birds on the East Coast of the United States (Kent, 2005) and lacustrine fish in North American lakes (Griffiths, 1997). A study was done on woody South American plants to show that biodiversity increases as precipitation levels increase (O'Brien, 1993). The Size-Complexity Rule can also be seen in island ecology where the number of herpetofauna to island area follows a power law (MacArthur & Wilson, 2001). The Size-Complexity Rule is often called species-area relationship in ecology literature. The same is seen in species richness on islands close to and further away from the mainland (Wilson & MacArthur, 1967) (Guo, 2015). This rule is also seen in the cumulative species number against cumulative transect area of breeding birds of the Talysh Mountains (Heiss, 2012). This is also seen in mammals, amphibians, and birds on a continental scale (Storch, Keil, & Jetz, 2012) as well as benthic macrofauna in 201 beaches around the world (McLachlan, 1990) (McLachlan, Jaramillo, Donn, & Wessels, 1993). Similarly, biological traits such as population density, population size, habitat specialization, and body size influence species-area relationships; thus size-complexity (KARLSON, 2006).

Our research aims to show how the Size-Complexity Rule can be expanded to include stellar systems, where this rule has not been applied thus far. We examine several implications of size-complexity in stars: progress of nucleosynthesis, average rate of nucleosynthesis, flow of nucleosynthesis, and efficiency. Progress of nucleosynthesis, P , is the ability of the star to group nucleons together into atoms and how much they are grouped, with how many other nucleons. The average rate of nucleosynthesis, η , is the rate of that the star combines nucleons together to form atoms from the star's initial formation to its super nova explosion. The flow of nucleosynthesis, ϕ , is the number of reactions the star performs in combining each singular nucleon to another to create each atom. The efficiency of the star, α , is its ability create elements over the course of its lifetime with the least amount of energy necessary to do so.

Our hypothesis is that stars with higher solar masses will have higher progress, average rate, flow, and efficiency nucleosynthesis yields and power trends than lower solar massed

stars. This is because higher massed stars are much hotter than lower massed stars, and the gravitational force of bigger stars is larger than smaller stars, which allows them to fuse more nucleons in their shorter life. We predict that a star's efficiency in grouping nucleons into more complicated elements increases as a function of their size since this is based on the Size-Complexity Rule, which states that a system's complexity is contingent to its size.

1.1 Quantity-Quality Transition

The Size-Complexity Rule is the Quantity-Quality Transition, recognized by the ancient Greeks. The Quantity-Quality transition is that the accumulation of quantity in a system, which is measured as the size of a system, causes changes in its quality, i.e. the structure and functioning of the system. Aristotle said that the Whole is greater than the sum of its parts (Aristotle & McMahon, 2018), which means that the increase of quantity in the whole, brings qualitative, emergent transformations and is not just additive. Hegel wrote about the quantity-quality in his work (Hegel, 2014). Dialectical Materialism also spent a great deal of attention on this transition (Jordan, 1967) (Thomas, 2009). Robert Carneiro wrote in 2000 (Carneiro, 2000) about the transition as a mechanism of social evolution. In many instances, people have been talking about those transitions without recognizing or naming them with different names. The species-area rule, or the species-population rules are some examples (Heiss, 2012) (Storch et al., 2012) (McLachlan et al., 1993) (KARLSON, 2006). Others are the number of occupations as function of the population, the number of different cells as a function of the total number of cells in an organism, the number of different ant castes as a function of the number of ants in the colony, etc. etc. (Bonner, 2004). There are two ways that complexity increase has been measured. One is the differentiation as a function of size, which are most of the above examples, and the other is the structure formation in the larger system as a result of this differentiation. For example, the number of different cells in an organism is one measure, but, it is correlated to the structure formation in organs and the overall functioning of the organism. For stellar evolution, the first step of the nucleosynthesis produces different kinds of atoms than the ones that existed before, and the larger the star is the more variety of atoms it can produce, but, on its turn, as in an organism, this differentiation leads to structure formation in the system as a whole, which for stars with larger variety of elements determines layered regions inside the star of different density, temperature, kinds of atoms and nuclear reactions occurring there. The specialization and differentiation in the existing elements leads to change in the global overall structure in a system, as observed in stars, organisms, cities, economies, etc.

2 Methods

This simulation is of large stars that explode as supernovae, and their composition can be compared with the measurements of the composition of already exploded stars (Suda et al., 2008).

The stellar yields of various isotopes, ranging from Hydrogen-1 to Gallium-71, were taken from 13, 15, 18, 20, 25, 30, and 40 solar massed stars with varying metallicities of 0, .001, .004, and .02. These yields of each isotope were given in solar masses from the SAGA Database (Suda et al., 2008) and (Nomoto et al., 2006). From the raw data of (Nomoto et al., 2006), the number of solar masses of each isotope from Hydrogen-1 to Gallium-71 and elements heavier than Gallium-71 present within each star at the end of its life was first converted to the total number of nucleons present within each star. We exclude the Hydrogen and Helium isotopes that existed before the star was formed when calculating the progress of nucleosynthesis and average rate of nucleosynthesis because those were not synthesized in the star, but part of the star's creation after the Big Bang. To determine the amount of Helium produced by the star from Hydrogen, we used Equation 1:

$$He_{nuc}[M_{\odot}] = \frac{\psi}{M_*} - .252 \quad (1)$$

where M_{\odot} is the solar mass of the Sun in kilograms, ψ is the sum of Helium-3 and Helium-4 in solar masses, and M_* is the total number of solar masses of a star. The total amount of Helium in each star was added together and divided by the total number of solar masses then subtracted from the fraction of Helium originally present immediately after the Big Bang (Wagoner, Fowler, & Hoyle, 1967) to find the fraction of the star made of nucleosynthesized helium from Hydrogen in solar masses. This number is reported as He_{nuc} , which is assigned a mass number of 4 since the majority of Helium present in the star has a mass number of 4. However, we did include the total number of Hydrogen and Helium isotopes when considering the calculated total number of nucleons present in each star because that is a measure of the size of the star.

We also included the elements heavier than Gallium-71 even though (Nomoto et al., 2006) excluded elements heavier than Gallium because those would have only measured trace amounts. To more accurately calculate the progress of nucleosynthesis, average rate of nucleosynthesis, flow, and efficiency of the star to make isotopes, the solar masses of elements heavier than Gallium-71 was calculated. Because the identity of these elements is not provided, the mass number of these is assumed to be 140 because that is approximately the mean mass number between naturally occurring Gallium and Uranium in the periodic system. These elements are referred to as "140- χ ." The total number of solar masses of 140- χ was calculated by subtracting the solar

masses of Hydrogen-1 to Gallium-71, the explosion energy in solar masses, and M_{cut} from the original number of solar masses of each star.

In the following calculations, we take into account the initial metallicity of the star and exclude those elements that were made by a previous star that would be incorporated into the stars of this study. Because these specific elements are not listed, we assume that they have a mass number of 100 and factor them into these calculations as "100- ρ ." To calculate the number of solar masses of 100- ρ , the initial metallicity of each star is multiplied by its M_* , its mass in solar masses.

To find the progress of nucleosynthesis and average rate of nucleosynthesis, we first calculated the number of nucleons of each isotope present in the star towards the end of its life using Equation 2 for each studied star with varying metallicities.

$$\beta_n = M_{\odot}[kg] \cdot M_{is}[M_{\odot}] \cdot 10^3 \left[\frac{g}{kg} \right] \cdot N_A \quad (2)$$

Where β_n is the synthesized number of nucleons of each isotope present in the star at the end of its life, M_{is} is the mass of the isotope present in the star in solar masses, and N_A is Avogadro's number. The values of each isotope from 0 metallicity stars are present in Table 1. The same is true for star sets with metallicities .001, .004, and .02 in Tables 2, 3, and 4, respectively.

We also calculated the initial total of nucleons present in each star, β_i , which is a measure of its size, or quantity, with equation 3:

$$\beta_i = M_{\odot}[kg] \cdot M_*[M_{\odot}] \cdot 10^3 \left[\frac{g}{kg} \right] \cdot N_A \quad (3)$$

where M_* is the mass of the star in solar masses. The initial total number of nucleons is shown in Table 5 and is the same for stars of the same solar mass despite the difference in initial metallicity.

We then multiplied the number of nucleons of each isotope from Nucleosynthesized Helium, 6-Li to 71-Ga, and 140- χ by its mass number, which is the number of nucleons of each individual isotope, to get ϵ_i , the progress of nucleosynthesis in an individual isotope, using equation 4:

$$\epsilon_i = \beta_n \cdot A \quad (4)$$

where A is the mass number of the isotope. We took the ϵ_i of each isotope of nucleosynthesized Helium, Lithium-6 to Gallium-71, and 140- χ and added them together. This number was subtracted from ϵ_{ρ} , the ϵ of 100- ρ , to get ϵ_{sum} , the total progress of nucleosynthesis within each star. Equation 5 shows this calculation. These values are recorded in Table 6.

$$\epsilon_{sum} = \epsilon_{He} + \sum_{i=6}^{71} \epsilon_i + \epsilon_{140} - \epsilon_{\rho} \quad (5)$$

The level of complexity of how far these stars went in grouping these nucleons together into heavier isotopes over their lifetime was also determined. The more connected the nucleons are, the more advanced the nucleosynthesis is in terms of the degree of complexity and progress of filling the periodic system of that star. The progress of nucleosynthesis for each star, P , is then determined by dividing ϵ_{sum} by the total number of nucleons in stars ranging from 13 to 40 M_* . This is seen in the Equation 6:

$$P = \frac{\epsilon_{sum}}{\beta_i} \quad (6)$$

The progress of nucleosynthesis was determined for each star when the metallicity equals 0, .001, .004, and .02 and reported in Table 8. The average rate of nucleosynthesis was determined by finding the lifetime of the star, τ , in equation 7 (Ryden, Peterson, & Demianski, 2010) :

$$\tau[10^{10} \text{ years}] = \frac{1}{M_*^2[M_{\odot}]} \quad (7)$$

where M_* is the number of solar masses of each star. Because these are heavy stars greater than 8 M_{\odot} , a power of 2 is used instead of 2.5. We then divided ϵ_{sum} by τ to find the average rate of nucleosynthesis, η , using equation 8:

$$\eta = \frac{\epsilon_{sum}}{\tau} \quad (8)$$

This equation calculates a rate measure for a star to group nucleons together over the course of its lifetime, τ . The average rate of nucleosynthesis was determined for each star of zero, 0.001, 0.004, and 0.02 initial metallicity and reported in Table 8.

Figure 1 was plotted to show the progress of nucleosynthesis vs. the initial number of M_* with initial metallicities equal to zero, 0.001, 0.004, and 0.02. Figure 2 was plotted to show the average rate of nucleosynthesis vs. the initial number of M_* with initial metallicities equal to zero, 0.001, 0.004, and 0.02.

2.1 Varying Explosion Energies

Then the stellar yields of various isotopes, ranging from Hydrogen-1 to Gallium-71, were taken from 20, 25, 30, and 40 solar mass stars with varying explosion energies and metallicities of 0, 0.001, 0.004, and 0.02. Stars with 20 and 25 solar masses have 10 E of explosion energy, where in all cases, $E \sim 1 \times 10^{51} \text{ ergs}$. 30 solar mass stars have 20E of explosion energy. Stars of 40 solar masses have explosion energies of 30E. These yields of each isotope were given in solar masses from the SAGA Database (Suda et al., 2008) and (Nomoto et al., 2006). The methods used for determining the P and η of varying metallicity stars are the same for when both the metallicity and explosion energy vary. The values of each isotope from 0 to 0.02 metallicity stars are

present in Tables 11, 12, 13, and 14. We also calculated the initial total number of nucleons present in each star, β_i and recorded the values in Table 15.

Table 16 listed the ϵ_{sum} of each star when the explosion energy varies the metallicity equals zero, 0.001, 0.004 and 0.02. The progress of nucleosynthesis is reported in Table 17, and the average rate of nucleosynthesis is reported in Table 18. The η of each star when explosion energies vary was determined for each star of zero to 0.02 initial metallicity and reported in Table 18.

3 Theory

In addition to finding the P and η of each star, in this Thesis paper we determine α , the action efficiency, of stars. α is defined by equation 9 from previous work (Georgiev et al., 2015) (Georgiev, Chatterjee, & Iannacchione, 2017):

$$\alpha = \frac{h \cdot z}{E \cdot t} = \frac{h \cdot \phi}{E[J] \cdot \tau[sec]} \quad (9)$$

where z is the number of events, h is the Planck's constant, t is the time in seconds, E is the kinetic energy used to combine each element in Joules per second, and ϕ is the number of nuclear combinations/formation of isotopes by adding one nucleon. ϕ is also called "Flow" in this Thesis paper. ϕ is calculated by first determining how many unique isotopes are formed from nucleosynthesis at the end of the star's life using the following equation:

$$\sigma_{iso} = \frac{\beta_n}{A} \quad (10)$$

where σ_{iso} is the number of atoms formed from grouping nucleons into an isotope. ϕ is found by combining each ϕ_{iso} for nucleosynthesized helium, 6-Li to 71-Ga, and 140- χ isotopes using Equations 11 and 12 :

$$\phi_{iso} = (A - 1) \cdot \sigma_{iso} \quad (11)$$

$$\phi = \phi_{He} + \sum_{i=6}^{71} \phi_i + \phi_{140} - \phi_p \quad (12)$$

where A is the mass number of the isotope, ϕ_i is the flow of isotopes from Lithium-6 to Gallium-71, and ϕ_p is the ϕ of 100- ρ . ϕ is the flow of events in the star over the course of its lifetime. The ϕ of each star is recorded in Tables 21 and 22. Equation 9 is rederived for stars in Equation 13 :

$$\alpha = \frac{h \cdot z}{E \cdot t} = \frac{h \cdot \phi}{(kL\tau) \cdot \tau} = \frac{h \cdot \phi}{(kL) \cdot \tau^2} = \frac{h \cdot \phi}{k \cdot M^3 \cdot (M^{-2})^2} \quad (13)$$

E is approximately the amount of energy absorbed by the star from the number of reactions that occurred in its lifetime. $kL\tau$ is equal to E . k is a constant of proportionality between the energy needed for nuclear reactions to occur in the star during its lifetime and the energy released through luminosity,

L . It is an energy fraction of L . Equation 14 describes this relationship:

$$k = \frac{E}{E_L} \quad (14)$$

where E_L is the total energy emitted by the luminosity. Because L is the luminosity, which is the energy it emits over time and equals M^3 , and $\tau = \frac{1}{M^2}$, this means that:

$$\alpha = \frac{h \cdot \phi}{k \cdot M^3 \cdot (M^{-2})^2} = \frac{h \cdot \phi}{k \cdot M^3 \cdot M^{-4}} = \frac{h \cdot \phi}{k \cdot M^{-1}} = hk^{-1} \phi M \quad (15)$$

This equation is used because it aids in showing if the principle of least action, the tendency of systems to become more efficient as their self-organization continues. Because k is a constant of proportionality, this paper calculates for αk .

$$\alpha k = h \phi M \quad (16)$$

Because α is determined using the number of nucleons that have been combined into a nucleus, M is substituted for β_i in the calculations for αk . The αk values in Tables 25 and 26.

3.1 Model

We consider the dependency between the characteristics of stellar evolution. The rate of progress and the degree of progress for each star, as well as its action efficiency are in a positive feedback with the mass of the star, or its total number of nucleons, which is the measure of the size of the star. This way the Size-Complexity Rule is expected here, where the larger the size of the star, the further it can go in grouping of the nucleons into heavier atoms, which is our measure of self-organization and complexity for nucleosynthesis and the faster the rate of self-organization. The size of the stars also determines the action efficiency for adding new nucleons, or for self-organizing of the elements.

4 Results

Tables 1, 2, 3, and 4 show the calculated number of nucleons for each isotope present in various massed stars of (Nomoto et al., 2006) when the initial metallicities equal zero, 0.001, 0.004, and 0.02 respectively. Table 5 shows the total number of nucleons of each star at the beginning of its life.

Table 6 shows the ϵ_{sum} of each star when only the metallicity varies. Table 7 shows the progress of nucleosynthesis within each star when the initial metallicity is zero, 0.001, 0.004, and 0.02 respectively. Figures 1 shows the progress of nucleosynthesis against the initial number of solar masses for each of these metallicities on a Log/Log scale at the end of the star's life. This shows that the progress of nucleosynthesis follow a power-law in stars even when their initial metallicities vary. Further, the advance in the progress of nucleosynthesis is relatively similar as the trend lines show.

Tables 8 the average rate of nucleosynthesis of each star over the star's lifetime when the initial metallicities equal zero, 0.001, 0.004, and 0.02 respectively. Figure 2 show the average rate of nucleosynthesis against the initial number of solar masses for each of these metallicities on a Log/Log scale at the end of each star's life. This shows that the average rate of nucleosynthesis follow a power-law in stars even when their initial metallicities vary. Further, the advance in the average rate of nucleosynthesis is relatively similar as the trend lines show.

Table 9 shows the coefficients, represented by c , and the powers, represented by y , for the equations of Figure 1 where the progress of nucleosynthesis is function of the initial number of nucleons. These equations follow the format:

$$P = c \cdot \beta_i^y \quad (17)$$

Table 10 shows the coefficients and the powers of the equations of Figure 2 where the average rate of nucleosynthesis is a function of the initial number of nucleons. These equations follow the format:

$$\eta = c \cdot \beta_i^y \quad (18)$$

Tables 11, 12, 13, and 14 show the calculated number of nucleons for each isotope present in various massed stars of (Nomoto et al., 2006) when the initial metallicities equal zero, 0.001, 0.004, and 0.02 respectively when the explosion energy varies. Table 15 shows the total number of nucleons of each star at the beginning of its life. Table 16 shows the ϵ_{sum} of each star when the explosion energy varies.

Table 17 show the progress of nucleosynthesis within each star when explosion energies vary and the initial metallicity is zero, 0.001, 0.004, and 0.02 respectively. Figure 3 shows the progress of nucleosynthesis against the initial number of nucleons for each of the given metallicities at their explosion energies on a Log/Log scale at the end of each star's life. This shows that the progress of nucleosynthesis follow a power-law in stars even when their initial metallicities vary. Further, the advance in the progress of nucleosynthesis is relatively similar as the trend lines show.

Table 18 shows the average rate of nucleosynthesis of each star over the star's lifetime when the initial metallicities equal zero, 0.001, 0.004, and 0.02. Figure 4 shows the average rate of nucleosynthesis against the initial number of nucleons for each of these metallicities on a Log/Log scale at the end of the star's life when their explosion energies vary. This shows that the average rate of nucleosynthesis follow a power-law in stars even when their initial metallicities vary. Further, the advance in the average rate of nucleosynthesis is relatively similar as the trend lines show.

Table 19 shows the coefficients and the powers of the equations of Figure 3 where the progress of nucleosynthesis is function of the initial number of nucleons. These equations follow the format of equation 17.

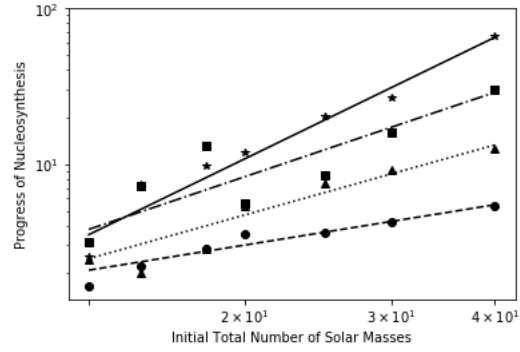


Figure 1. is the combined data of the progress of nucleosynthesis vs. the initial total number of nucleons on a Log/Log scale. The "·" points are the markers for stars with initial metallicities equal to 0, and the trend line of these points is represented as a "· · ·" line. The triangular points are the markers for stars with initial metallicities of 0.001, and the trend line is represented by a "· · ·" line. The square points are markers for stars with initial metallicities of 0.004, and the trend line is represented by a "· · ·" line. The "*" points are markers for stars with initial metallicities equals to 0.02, and these have a solid black trend line.

Table 20 shows the coefficients and the powers of the equations of Figure 4 where the average rate of nucleosynthesis is a function of the initial number of nucleons. These equations follow the format of equation 18.

Tables 21 and 22 report the flow values over each star. Figures 5 and 6 show the total ϕ of each star over their initial number of solar masses. Tables 23 and 24 report the coefficients and powers of each metallicity star in the following format:

$$\phi = c \cdot \beta_i^y \quad (19)$$

where c is the coefficient and y is the power for flow. These show that the flow of nucleosynthesis follows a power-law in stars even when their initial metallicities and explosion energies vary. Further, the advance in the flow rate of nucleosynthesis is relatively similar as the trend lines show.

Tables 25 and 26 report the alpha values for each star. Figures 7 and 8 show the total α of each star versus their initial number of solar masses. The data for each metallicity star follows a power law, as shown by the trend line, and shows that the efficiency of stars to create elements increases as their individual size is larger. This trend is seen in stars that have the same explosion energy and varying explosion energies. The trends of Figures 7 and 8 are reported in Tables 27 and 28 in the following format:

$$\alpha k = c \cdot \beta_i^y \quad (20)$$

where c is the coefficient and y is the power for α .

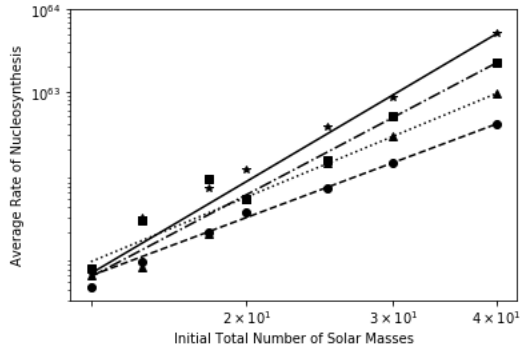


Figure 2. is the combined data of the average rate of nucleosynthesis vs. the initial total number of nucleons on a Log/Log scale. The ". ." points are the markers for stars with initial metallicities equal to 0, and the trend line of these points is represented as a "----" line. The triangular points are the markers for stars with initial metallicities of 0.001, and the trend line is represented by a "..." line. The square points are markers for stars with initial metallicities of 0.004, and the trend line is represented by a "-.-" line. The "*" points are markers for stars with initial metallicities equals to 0.02, and these have a solid black trend line.

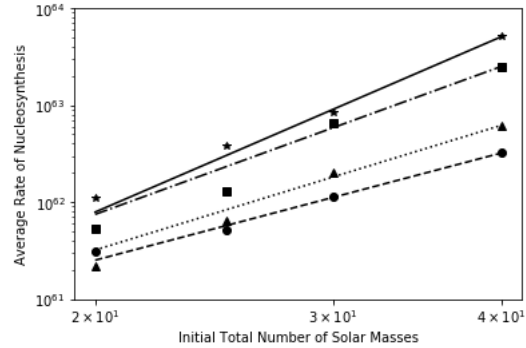


Figure 4. is the combined data of the average rate of nucleosynthesis vs. the initial total number of nucleons on a Log/Log scale when the explosion energies vary. The ". ." points are the markers for stars with initial metallicities equal to 0, and the trend line of these points is represented as a "----" line. The triangular points are the markers for stars with initial metallicities of 0.001, and the trend line is represented by a "..." line. The square points are markers for stars with initial metallicities of 0.004, and the trend line is represented by a "-.-" line. The "*" points are markers for stars with initial metallicities equals to 0.02, and these have a solid black trend line.

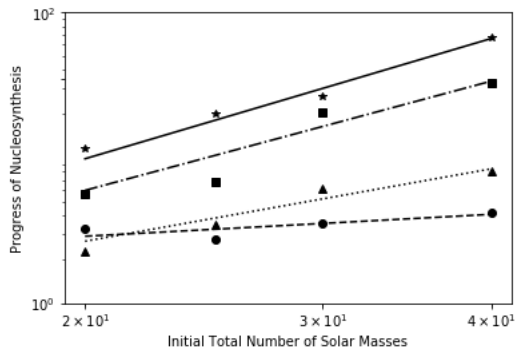


Figure 3. is the combined data of the progress of nucleosynthesis vs. the initial total number of nucleons on a Log/Log scale when the explosion energies vary. The ". ." points are the markers for stars with initial metallicities equal to 0, and the trend line of these points is represented as a "----" line. The triangular points are the markers for stars with initial metallicities of 0.001, and the trend line is represented by a "..." line. The square points are markers for stars with initial metallicities of 0.004, and the trend line is represented by a "-.-" line. The "*" points are markers for stars with initial metallicities equals to 0.02, and these have a solid black trend line.

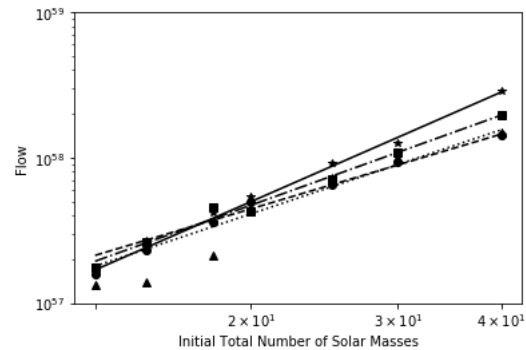


Figure 5. is the combined data of the flow of nucleosynthesis vs. the initial total number of nucleons on a Log/Log scale when only the metallicity varies. The ". ." points are the markers for stars with initial metallicities equal to 0, and the trend line of these points is represented as a "----" line. The triangular points are the markers for stars with initial metallicities of 0.001, and the trend line is represented by a "..." line. The square points are markers for stars with initial metallicities of 0.004, and the trend line is represented by a "-.-" line. The "*" points are markers for stars with initial metallicities equals to 0.02, and these have a solid black trend line.

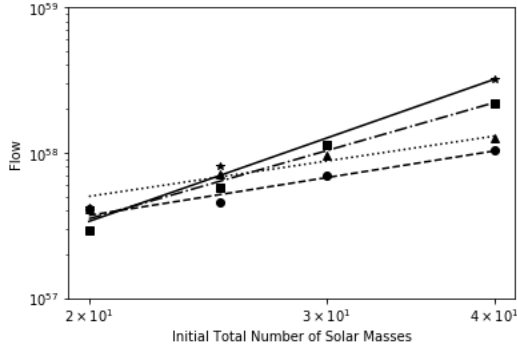


Figure 6. is the combined data of the flow of nucleosynthesis vs. the initial total number of nucleons on a Log/Log scale when the explosion energy varies. The "·" points are the markers for stars with initial metallicities equal to 0, and the trend line of these points is represented as a "---" line. The triangular points are the markers for stars with initial metallicities of 0.001, and the trend line is represented by a "... " line. The square points are markers for stars with initial metallicities of 0.004, and the trend line is represented by a "- · -" line. The "*" points are markers for stars with initial metallicities equals to 0.02, and these have a solid black trend line.

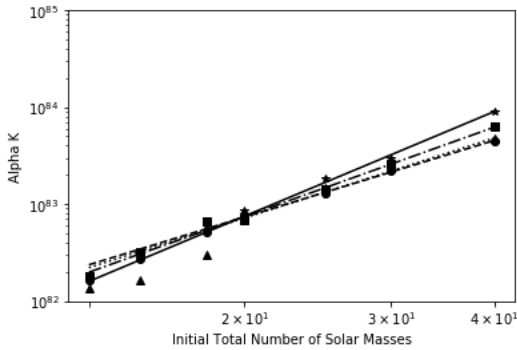


Figure 7. is the graphed relationship between the αk versus the initial total number of nucleons on a Log/Log scale for all sized stars studied. The "·" points are the markers for stars with initial metallicities equal to 0, and the trend line of these points is represented as a "---" line. The triangular points are the markers for stars with initial metallicities of 0.001, and the trend line is represented by a "... " line. The square points are markers for stars with initial metallicities of 0.004, and the trend line is represented by a "- · -" line. The "*" points are markers for stars with initial metallicities equals to 0.02, and these have a solid black trend line.

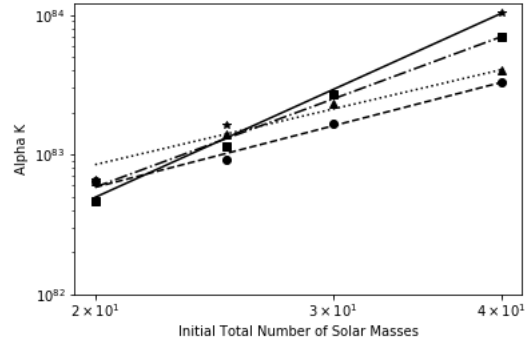


Figure 8. is the graphed relationship between the αk versus the initial total number of nucleons on a Log/Log scale for all sized stars when the explosion energy varies. The "·" points are the markers for stars with initial metallicities equal to 0, and the trend line of these points is represented as a "---" line. The triangular points are the markers for stars with initial metallicities of 0.001, and the trend line is represented by a "... " line. The square points are markers for stars with initial metallicities of 0.004, and the trend line is represented by a "- · -" line. The "*" points are markers for stars with initial metallicities equals to 0.02, and these have a solid black trend line.

5 Discussion

We found the number of nucleons in each star by multiplying its mass times the Avogadro's number, and then multiplied times the mass fraction of heavier elements.

Figure 1 further shows that despite the variation in the initial metallicity of the star, its progress of nucleosynthesis increases when the size of the star increases. Figure 1 suggests that the progress of nucleosynthesis follows a power-law regardless of initial metallicity of the stars. The same can be said for Figure 3 when explosion energies vary among stars.

Figure 2 shows that stars, despite their difference in initial metallicity, the average rate of nucleosynthesis increases as their initial size increases. Figure 4 also shows that the average rate of nucleosynthesis in stars follows a power-law relationship. This power-law is also seen in the flow trends of Figures 5 and 6 of these stars. The α of each star also follows this trend, as suggested by Figures 7 and 8, since the α increases as the initial number of nucleons increases. Action efficiency is larger in stars that bigger than in smaller stars, which agrees with our hypothesis.

This means that the level of complexity is more advanced in higher massed stars than in lower massed stars similar to (Bonner, 2004) and (Georgiev et al., 2015) as they show that the larger a system is the more complex it is, and it happens more action efficiently as given by the rate. As the number of nucleons increases, the larger the rate of nucleosynthesis is, i.e. higher action efficiency, as predicted by LAP

and variational calculus. Further, as suggested by Figure 2 and 4, this trend also shows that an increase in the rate of nucleosynthesis in larger stars follows a power-law, as predicted by the model. Our data suggests that since the complexity of the higher massed stars increases, the average rate of nucleosynthesis also increases, and this is true even when metallicities differ. This makes sense because reaction rates of nucleosynthesis are highly temperature dependent. Because larger stars are hotter than smaller stars, and the flow of stars increases with size, the average rate of nucleosynthesis and action efficiency would be higher in larger stars than smaller stars. Figures 7 and 8 shows that stars with larger solar masses/ initial number of nucleons are more action efficient than smaller stars. All trends in this Thesis paper follow a power-law, which means that stars follow a similar trend to the past research in the level complexity of CPUs (Georgiev et al., 2015) and other works by Bonner (Bonner, 2004).

However, possible limitations to our research include how there is no reported data on when nucleosynthesis takes place in stars (Nomoto et al., 2006). Because of this, we could only report the overall average rate of nucleosynthesis and progress of nucleosynthesis for each star. Other limitations can include how since more advanced elements, larger than Gallium-71, were not reported in (Nomoto et al., 2006), we used approximate numbers for their mass numbers by assuming it was 140. While we take into account the fraction of the star that was not made by that star specifically, we also had to assume that the mass number of this fraction is a median mass number between Hydrogen and Uranium in the periodic system, 100. Also, there are a total of four points in the graphs describing trends in stars with varying explosion energy, compared to the seven points in graphs that do not describe trends in these types of star. This is because (Nomoto et al., 2006) excludes 13 to 18 solar massed stars from their yields tables when the explosion energy varies.

Future work should look into the value of k . This constant cannot be equal to 1 because that would imply that all energy used in the nuclear reactions was used, and no luminosity energy was released. It is possible that the value of k is proportional to the mass of the star because:

$$E_L = L[J/sec] \cdot \tau = M^3 \cdot \frac{1}{M^2} = M \quad (21)$$

We believe that k is equal to 0.01. Future tests should determine whether the k value is found from an equation and if these values also follow a power law. Further, because heavier stars increase in metallicity by a power law, future experiments should look into using the explosion energy of each star for calculating α . This is because more advanced elements are formed after a super nova event. The following equation should be used:

$$E_{tot} = kE_L + k_1E_{exp} \quad (22)$$

E_{tot} is the total energy used to synthesize the isotopes, k_1 is the energy fraction from the luminosity of the explosion, and E_{exp} is the energy of the explosion.

6 Conclusion

In this Thesis paper, we have studied the progress, average rate, flow, and action efficiency of nucleosynthesis in stellar evolution for stars of different mass and initial metallicity in order to compare it with the rates of organization increase in other systems. We consider stars as complex systems, and one measure of their complexity is the degree to which they combined nucleons into heavier elements. The more of the heavier element there is as a fraction of the mass of the star, the more advanced it is in its evolutionary stage and degree of complexity. We chose simulations by (Nomoto et al., 2006) of stars of different masses and metallicities at the end of their life, when they have exploded as supernovae and their composition can be detected by spectral analysis of their nebulae. Those simulations were checked against observations of already exploded stars in the SAGA catalog (Suda et al., 2008). By calculating the stellar lifetime, using the mass of each star, we were able to find the average rate of nucleosynthesis over their lifetime including the explosion, which tells us about action efficiency. Additionally, finding flow for each star helps tell us about the action efficiency of the system by showing how more nuclear combinations occur over a shorter lifetime. Only stars of mass larger than eight solar masses explode as supernovae, that is why there are no data for less massive stars. This is a measure of the average rate of increase of the increase of complexity of each star. We found that the progress, average rates, flow, and action efficiency are in a power law dependence on the mass of the star and correspondingly of the number of nucleons even when the initial metallicity and explosion energies are different. This compares to our previous studies in CPUs evolution, where all of their characters showed to be power laws of each other. This shows that the larger the star is, the faster it advances in its progress, average rate, flow, and action efficiency of nucleosynthesis as a measure for its level of complexity, and this dependency is a power law, similar to previous studies of Size-Complexity Rules (Bonner, 2004) and in our own studies of CPU systems. The goal is to show that this power law dependence is a universal feature of all complex systems, independent of their nature, physical, chemical, biological, technological, social, etc., and to apply it in our future work to as many other systems as possible to look for confirmations of this rule and for possible exceptions. In order to show the applicability of first principles, and of the Principle and Least Action and action efficiency importance in this research, we are planning to look for the time dependence of the rate of nucleosynthesis during the lifetime in each individual star.

Acknowledgement

We would like to thank the Assumption College Honor's Program and the department of Natural Sciences for financial support, as well as Assumption students Thanh Vu, Simon Trcka and Lamberto Qako for help with data collection. We would also like to thank Assumption students Nicole Bramlitt and Rebecca Gilchrist for long discussions and for proof-reading the paper.

References

- Amado, A., Batista, C., & Campos, P. R. (2018). A theoretical approach to the size-complexity rule. *Evolution*, 72(1), 18–29.
- Aristotle, & McMahon, J. H. (2018). *The metaphysics*. Dover Publications, Inc.
- Bell, G., & Mooers, A. O. (1997). Size and complexity among multicellular organisms. *Biological Journal of the Linnean Society*, 60(3), 345–363.
- Bonner, J. T. (1993). Dividing the labour in cells and societies. *Current science*, 64(7), 459–466.
- Bonner, J. T. (1995). The evolution of life's complexity. *Nature*, 374(6522), 508–509.
- Bonner, J. T. (2004). Perspective: the size-complexity rule. *Evolution*, 58(9), 1883–1890.
- Bonner, J. T. (2015). *Size and cycle: an essay on the structure of biology* (Vol. 2087). Princeton University Press.
- Carneiro, R. L. (2000). The transition from quantity to quality: A neglected causal mechanism in accounting for social evolution. *Proceedings of the National Academy of Sciences*, 97(23), 12926–12931.
- Cockburn, D., Crabtree, S. A., Kobti, Z., Kohler, T. A., & Bocinsky, R. K. (2013). Simulating social and economic specialization in small-scale agricultural societies. *Journal of Artificial Societies and Social Simulation*, 16(4), 4.
- Curtis, S., Ebinger, K., Fröhlich, C., Hempel, M., Perego, A., Liebendörfer, M., & Thielemann, F.-K. (2018). Pushing core-collapse supernovae to explosions in spherical symmetry. iii. nucleosynthesis yields. *The Astrophysical Journal*, 870(1), 2.
- Finlay, B. J., & Esteban, G. F. (2009). Can biological complexity be rationalized? *BioScience*, 59(4), 333–340.
- Frebel, A., Aoki, W., Christlieb, N., Ando, H., Asplund, M., Barklem, P. S., ... others (2005). Nucleosynthetic signatures of the first stars. *Nature*, 434(7035), 871.
- Frebel, A., Norris, J. E., Aoki, W., Honda, S., Bessell, M. S., Takada-Hidai, M., ... Christlieb, N. (2007). Chemical abundance analysis of the extremely metal-poor star he 1300+ 0157. *The Astrophysical Journal*, 658(1), 534.
- Gaston, K. J. (2000). Global patterns in biodiversity. *Nature*, 405(6783), 220.
- Georgiev, G. Y., Chatterjee, A., & Iannacchione, G. (2017). Exponential self-organization and moore's law: Measures and mechanisms. *Complexity*, 2017.
- Georgiev, G. Y., Henry, K., Bates, T., Gombos, E., Casey, A., Daly, M., ... Lee, H. (2015). Mechanism of organization increase in complex systems. *Complexity*, 21(2), 18–28.
- Griffiths, D. (1997). Local and regional species richness in north american lacustrine fish. *Journal of Animal Ecology*, 49–56.
- Guo, Q. (2015). Island biogeography theory: emerging patterns and human effects. *Earth Systems and Environmental Sciences* 5 p., 32(1), 1–5.
- Hall, R. H., Johnson, N. J., & Haas, J. E. (1967). Organizational size, complexity, and formalization. *American Sociological Review*, 903–912.
- Hegel, G. W. F. (2014). *Georg wilhelm friedrich hegel: the science of logic*. Cambridge University Press.
- Heim, N. A., Payne, J. L., Finnegan, S., Knope, M. L., Kowalewski, M., Lyons, S. K., ... Wang, S. C. (2017). Hierarchical complexity and the size limits of life. *Proceedings of the Royal Society B: Biological Sciences*, 284(1857), 20171039.
- Heiss, M. (2012). Impact of forest degradation on breeding birds of the talysh mountains in the azerbaijan republic. *Journal homepage: www.wesca.net*, 7(1/2).
- Holbrook, C. T., Barden, P. M., & Fewell, J. H. (2011). Division of labor increases with colony size in the harvester ant *pogonomyrmex californicus*. *Behavioral Ecology*, 22(5), 960–966.
- Johnson, C. I., & Pilachowski, C. A. (2010, sep). CHEMICAL ABUNDANCES FOR 855 GIANTS IN THE GLOBULAR CLUSTER OMEGA CENTAURI (NGC 5139). *The Astrophysical Journal*, 722(2), 1373–1410. Retrieved from
- Jordan, Z. A. (1967). *The evolution of dialectical materialism*. Macmillan.
- KARLSON, R. H. (2006). Metapopulation dynamics and community ecology of marine systems. In *Marine metapopulations* (pp. 457–489). Elsevier.
- Kent, M. (2005). Biogeography and macroecology. *Progress in Physical Geography*, 29(2), 256–264.
- MacArthur, R. H., & Wilson, E. O. (2001). *The theory of island biogeography* (Vol. 1). Princeton university press.
- McGlenn, D. J., Xiao, X., May, F., Gotelli, N. J., Engel, T., Blowes, S. A., ... McGill, B. J. (2019). Measurement of biodiversity (mob): A method to separate the scale-dependent effects of species abundance distribution, density, and aggregation on diversity change. *Methods in Ecology and Evolution*, 10(2), 258–269.
- McLachlan, A. (1990). Dissipative beaches and macrofauna communities on exposed intertidal sands. *Journal of coastal research*, 57–71.
- McLachlan, A., Jaramillo, E., Donn, T. E., & Wessels, F. (1993). Sandy beach macrofauna communities and their control by the physical environment: a geographical comparison. *Journal of Coastal Research*, 27–38.
- Mori, K., Famiano, M. A., Kajino, T., Suzuki, T., Garnavich, P. M., Mathews, G. J., ... Nomoto, K. (2018). Nucleosynthesis constraints on the explosion mechanism for type ia supernovae. *The Astrophysical Journal*, 863(2), 176.
- Nomoto, K. (2016). First stars, hypernovae, and superluminous supernovae. *International Journal of Modern Physics D*, 25(10), 1630025.
- Nomoto, K., Hashimoto, M., Tsujimoto, T., Thielemann, F.-K., Kishimoto, N., Kubo, Y., & Nakasato, N. (1997). Nucleosynthesis in type ii supernovae. *Nuclear Physics A*, 616(1-2), 79–90.
- Nomoto, K., Kobayashi, C., & Tominaga, N. (2013). Nucleosynthesis in stars and the chemical enrichment of galaxies. *Annual Review of Astronomy and Astrophysics*, 51, 457–509.

- Nomoto, K., & Suzuki, T. (2013). Supernova yields for chemical evolution modeling. *Proceedings of the International Astronomical Union*, 9(S298), 154–166.
- Nomoto, K., Tominaga, N., Umeda, H., & Kobayashi, C. (2005). Yields of population iii supernovae and the abundance patterns of extremely metal-poor stars. *Proceedings of the International Astronomical Union*, 1(S228), 287–296.
- Nomoto, K., Tominaga, N., Umeda, H., Kobayashi, C., & Maeda, K. (2006). Nucleosynthesis yields of core-collapse supernovae and hypernovae, and galactic chemical evolution. *Nuclear Physics A*, 777, 424–458.
- O’Brien, E. M. (1993). Climatic gradients in woody plant species richness: towards an explanation based on an analysis of southern africa’s woody flora. *Journal of Biogeography*, 181–198.
- Pignatari, M., Herwig, F., Hirschi, R., Bennett, M., Rockefeller, G., Fryer, C., ... others (2016). Nugrid stellar data set. i. stellar yields from h to bi for stars with metallicities $z=0.02$ and $z=0.01$. *The Astrophysical Journal Supplement Series*, 225(2), 24.
- Prantzos, N., Abia, C., Limongi, M., Chieffi, A., & Cristallo, S. (2018). Chemical evolution with rotating massive star yields—i. the solar neighbourhood and the s-process elements. *Monthly Notices of the Royal Astronomical Society*, 476(3), 3432–3459.
- Ritter, C., Herwig, F., Jones, S., Pignatari, M., Fryer, C., & Hirschi, R. (2018). Nugrid stellar data set—ii. stellar yields from h to bi for stellar models with $m_{\text{zams}}=1\text{--}25\text{ }M_{\odot}$ and $z=0.0001\text{--}0.02$. *Monthly Notices of the Royal Astronomical Society*, 480(1), 538–571.
- Rosenzweig, M. L., et al. (1995). *Species diversity in space and time*. Cambridge University Press.
- Ryden, B. S., Peterson, B. M., & Demianski, M. (2010). *Foundations of astrophysics* (Vol. 489). Addison-Wesley.
- Sinha, S., Fröhlich, C., Ebinger, K., Perego, A., Hempel, M., Eichler, M., ... Thielemann, F.-K. (2017). Pushing core-collapse supernovae to explosions in spherical symmetry: nucleosynthesis yields. In *Proceedings of the 14th international symposium on nuclei in the cosmos (nic2016)* (p. 020608).
- Steigman, G. (2007). Primordial nucleosynthesis in the precision cosmology era. *Annu. Rev. Nucl. Part. Sci.*, 57, 463–491.
- Storch, D., Keil, P., & Jetz, W. (2012). Universal species–area and endemics–area relationships at continental scales. *Nature*, 488(7409), 78.
- Suda, T., Katsuta, Y., Yamada, S., Suwa, T., Ishizuka, C., Komiya, Y., ... Fujimoto, M. Y. (2008). Stellar abundances for the galactic archeology (saga) database—compilation of the characteristics of known extremely metal-poor stars. *Publications of the Astronomical Society of Japan*, 60(5), 1159–1171.
- Takahashi, K., Umeda, H., & Yoshida, T. (2014). Stellar yields of rotating first stars. i. yields of weak supernovae and abundances of carbon-enhanced hyper-metal-poor stars. *The Astrophysical Journal*, 794(1), 40.
- Thielemann, F.-K., Diehl, R., Heger, A., Hirschi, R., & Liebendörfer, M. (2018). Massive stars and their supernovae. In *Astrophysics with radioactive isotopes* (pp. 173–286). Springer.
- Thomas, P. (2009). *Marxism and scientific socialism: from engels to althusser*. Routledge.
- Tominaga, N., Iwamoto, N., & Nomoto, K. (2014). Abundance profiling of extremely metal-poor stars and supernova properties in the early universe. *The Astrophysical Journal*, 785(2), 98.
- Umeda, H., & Nomoto, K. (2003). First-generation black-hole-forming supernovae and the metal abundance pattern of a very iron-poor star. *Nature*, 422(6934), 871.
- Wagoner, R. V., Fowler, W. A., & Hoyle, F. (1967). On the synthesis of elements at very high temperatures. *The Astrophysical Journal*, 148, 3.
- Wanajo, S., Nomoto, K., Janka, H.-T., Kitaura, F., & Müller, B. (2009). Nucleosynthesis in electron capture supernovae of asymptotic giant branch stars. *The Astrophysical Journal*, 695(1), 208.
- Wilson, E. O., & MacArthur, R. H. (1967). The theory of island biogeography. *Princeton, NJ*.

Table 1
Calculated Number of Nucleons of Each Isotope when the Metallicity Equals Zero

$M_*(M_\odot)$	13	15	18	20	25	30	40
p	7.89×10^{57}	9.08×10^{57}	1.01×10^{58}	1.05×10^{58}	1.27×10^{58}	1.4×10^{58}	1.68×10^{58}
d	1.78×10^{41}	2.02×10^{41}	1.53×10^{41}	1.04×10^{41}	2.42×10^{41}	1.61×10^{41}	4.14×10^{41}
3-He	4.93×10^{52}	4.9×10^{52}	3.99×10^{52}	5.7×10^{52}	2.53×10^{53}	2.47×10^{53}	3.07×10^{52}
4-He	4.8×10^{57}	5.27×10^{57}	6.49×10^{57}	7.11×10^{57}	9.62×10^{57}	1.14×10^{58}	1.43×10^{58}
$H_{e_{nuc}}$	8.79×10^{56}	7.43×10^{56}	1.06×10^{57}	1.08×10^{57}	2.07×10^{57}	2.35×10^{57}	2.18×10^{57}
6-Li	4.37×10^{34}	1.33×10^{35}	5.23×10^{34}	4.37×10^{36}	3.22×10^{36}	1.35×10^{35}	9.03×10^{35}
7-Li	2.6×10^{47}	3.52×10^{47}	8.79×10^{46}	3.34×10^{47}	6.8×10^{48}	2.83×10^{49}	4.5×10^{46}
9-Be	2.12×10^{37}	3.86×10^{35}	1.26×10^{35}	5.38×10^{34}	1.49×10^{40}	1.51×10^{37}	6.38×10^{37}
10-B	3.5×10^{36}	9.94×10^{37}	4.7×10^{36}	1.88×10^{38}	3.44×10^{39}	6.2×10^{37}	2.84×10^{40}
11-B	3.52×10^{41}	3.95×10^{41}	8.55×10^{41}	7.83×10^{40}	1.13×10^{42}	3.92×10^{42}	3.68×10^{43}
12-C	8.88×10^{55}	2.06×10^{56}	2.61×10^{56}	2.53×10^{56}	3.52×10^{56}	4.04×10^{56}	5.14×10^{56}
13-C	1×10^{50}	7.44×10^{49}	3.15×10^{48}	1.37×10^{49}	1.76×10^{49}	1.22×10^{49}	3.84×10^{48}
14-N	2.19×10^{54}	2.23×10^{54}	2.26×10^{53}	6.49×10^{52}	7.08×10^{53}	1.96×10^{51}	7.05×10^{50}
15-N	7.64×10^{49}	8.22×10^{49}	2.87×10^{49}	1.35×10^{49}	1.4×10^{50}	2×10^{49}	7.53×10^{50}
16-O	5.39×10^{56}	9.26×10^{56}	1.65×10^{57}	2.53×10^{57}	3.34×10^{57}	5.76×10^{57}	1×10^{58}
17-O	2.02×10^{51}	1.88×10^{51}	3.34×10^{50}	8.18×10^{49}	1.78×10^{51}	2.25×10^{49}	1.7×10^{48}
18-O	6.94×10^{49}	5.86×10^{51}	5.55×10^{51}	3.02×10^{49}	8.08×10^{50}	2.47×10^{48}	2.55×10^{50}
19-F	1.4×10^{47}	2.36×10^{48}	9.47×10^{48}	1.94×10^{48}	2.05×10^{48}	1.07×10^{48}	2.85×10^{47}
20-Ne	1.83×10^{55}	3.92×10^{56}	5.92×10^{56}	1.09×10^{57}	6.38×10^{56}	1.02×10^{57}	3.68×10^{56}
21-Ne	6.49×10^{50}	4.5×10^{52}	1.09×10^{53}	5.15×10^{52}	1.59×10^{52}	6.6×10^{52}	1.29×10^{52}
22-Ne	2.37×10^{50}	1.93×10^{52}	3.08×10^{52}	8.29×10^{52}	2.42×10^{52}	1.03×10^{53}	8.08×10^{51}
23-Na	1.72×10^{53}	2.93×10^{54}	2.49×10^{54}	3.47×10^{54}	1.23×10^{54}	1.7×10^{54}	2.2×10^{53}
24-Mg	1.03×10^{56}	8.17×10^{55}	1.88×10^{56}	1.8×10^{56}	1.44×10^{56}	2.71×10^{56}	5.73×10^{56}
25-Mg	1.87×10^{53}	3.57×10^{53}	6.98×10^{53}	1.39×10^{53}	4.76×10^{52}	2.92×10^{53}	5.13×10^{53}
26-Mg	8.47×10^{52}	4.77×10^{53}	1.05×10^{54}	2.85×10^{53}	6×10^{52}	1.55×10^{53}	1.5×10^{53}
26-Al	1.19×10^{51}	1.33×10^{51}	3.99×10^{51}	5.96×10^{50}	8.98×10^{50}	3.5×10^{51}	1.66×10^{51}
27-Al	4.53×10^{54}	1.64×10^{54}	3.76×10^{54}	1.64×10^{54}	9.68×10^{53}	3.15×10^{54}	1.76×10^{55}
28-Si	9.63×10^{55}	8.77×10^{55}	1.39×10^{56}	1.19×10^{56}	4.2×10^{56}	2.97×10^{56}	1.22×10^{57}
29-Si	8.98×10^{53}	2.86×10^{53}	5.29×10^{53}	2.18×10^{53}	3.25×10^{53}	7.04×10^{53}	3.11×10^{54}
30-Si	1.7×10^{54}	1.78×10^{53}	4.13×10^{53}	1.32×10^{53}	9.03×10^{52}	3.05×10^{53}	4.86×10^{54}
31-P	5.85×10^{53}	6.74×10^{52}	1.58×10^{53}	9.59×10^{52}	1.01×10^{53}	1.4×10^{53}	1.92×10^{54}
32-S	2.84×10^{55}	3.83×10^{55}	4.87×10^{55}	6.36×10^{55}	2.22×10^{56}	1.39×10^{56}	4.47×10^{56}
33-S	1.08×10^{53}	9.04×10^{52}	1.23×10^{53}	2.37×10^{53}	3.28×10^{53}	1.98×10^{53}	9.7×10^{53}
34-S	3.34×10^{53}	2.42×10^{53}	3.41×10^{53}	5.87×10^{53}	5.08×10^{53}	1.01×10^{53}	1.9×10^{54}
36-S	1.77×10^{49}	1.71×10^{48}	6.4×10^{48}	3.07×10^{48}	4.08×10^{47}	8.43×10^{47}	3.82×10^{49}
35-Cl	6.56×10^{52}	1.75×10^{52}	3.16×10^{52}	8.24×10^{52}	6.49×10^{52}	2.75×10^{52}	2.59×10^{53}
37-Cl	3.64×10^{51}	6.98×10^{51}	1.09×10^{52}	4.62×10^{52}	7.32×10^{52}	1.84×10^{52}	1.16×10^{53}
36-Ar	3.88×10^{54}	6.32×10^{54}	6.79×10^{54}	1.16×10^{55}	3.71×10^{55}	2.35×10^{55}	5.83×10^{55}
38-Ar	6.26×10^{52}	7.46×10^{52}	2.04×10^{53}	4.62×10^{53}	4.3×10^{53}	4.17×10^{52}	1.33×10^{54}
40-Ar	9.59×10^{46}	2.13×10^{46}	4.74×10^{46}	1.27×10^{47}	2.12×10^{46}	5.58×10^{45}	1.55×10^{47}
39-K	6.01×10^{51}	9.41×10^{51}	2.31×10^{52}	5.27×10^{52}	7.55×10^{52}	1.56×10^{52}	1.41×10^{53}
40-K	1.37×10^{48}	1.09×10^{48}	2.35×10^{48}	1.56×10^{49}	9.63×10^{48}	1.19×10^{48}	1.25×10^{49}
41-K	4.24×10^{50}	9.64×10^{50}	2.06×10^{51}	1.13×10^{52}	2.49×10^{52}	4.06×10^{51}	3.35×10^{52}
40-Ca	3.5×10^{54}	5.28×10^{54}	5.27×10^{54}	7.45×10^{54}	2.97×10^{55}	2.08×10^{55}	4.47×10^{55}
42-Ca	1.17×10^{51}	1.47×10^{51}	4.34×10^{51}	1.53×10^{52}	8.94×10^{51}	1.03×10^{51}	2.6×10^{52}
43-Ca	7.74×10^{49}	5.91×10^{49}	4.06×10^{49}	8.9×10^{49}	1.89×10^{49}	2.31×10^{48}	1.16×10^{49}
44-Ca	2.01×10^{52}	2.65×10^{52}	1.74×10^{52}	1.74×10^{52}	1.17×10^{52}	6.52×10^{51}	1.04×10^{52}
46-Ca	1.28×10^{45}	2.11×10^{45}	1.11×10^{46}	1.56×10^{47}	3.33×10^{46}	7.25×10^{44}	6.23×10^{45}
48-Ca	1.86×10^{40}	5.04×10^{43}	4.93×10^{41}	5.27×10^{41}	1.51×10^{46}	4.25×10^{41}	1.56×10^{40}
45-Sc	2.54×10^{49}	4.83×10^{49}	6.64×10^{49}	3.05×10^{50}	7.38×10^{50}	1.81×10^{50}	6.96×10^{50}

46-Ti	7.52×10^{51}	3.25×10^{51}	4.86×10^{51}	7.16×10^{51}	3.81×10^{51}	6.32×10^{50}	1.29×10^{52}
47-Ti	1.05×10^{52}	4.62×10^{51}	6.35×10^{51}	5.1×10^{51}	7.07×10^{49}	4.55×10^{49}	1.11×10^{50}
48-Ti	7.59×10^{52}	1×10^{53}	9.16×10^{52}	1.06×10^{53}	1.86×10^{53}	2.16×10^{53}	2.93×10^{53}
49-Ti	2.72×10^{51}	3.98×10^{51}	3.59×10^{51}	4.72×10^{51}	8.43×10^{51}	1.06×10^{52}	1.44×10^{52}
50-Ti	1.41×10^{45}	1.14×10^{45}	2.06×10^{45}	2.19×10^{45}	2.68×10^{45}	5.5×10^{43}	1.13×10^{46}
50-V	1.62×10^{46}	1.26×10^{46}	5.51×10^{46}	1.63×10^{47}	1.4×10^{47}	3.16×10^{45}	7.82×10^{47}
51-V	1.98×10^{52}	1.29×10^{52}	1.49×10^{52}	1.32×10^{52}	1.08×10^{52}	1.27×10^{52}	2.11×10^{52}
50-Cr	1.25×10^{52}	1.86×10^{52}	3.16×10^{52}	2.66×10^{52}	5.85×10^{52}	4.58×10^{52}	2.13×10^{53}
52-Cr	1.05×10^{54}	1.31×10^{54}	1.35×10^{54}	1.63×10^{54}	3.32×10^{54}	3.74×10^{54}	4.73×10^{54}
53-Cr	5.94×10^{52}	8.1×10^{52}	7.7×10^{52}	9.92×10^{52}	1.8×10^{53}	2.18×10^{53}	3.13×10^{53}
54-Cr	2.81×10^{47}	4.95×10^{47}	3.89×10^{48}	3.81×10^{48}	1.12×10^{49}	2.06×10^{47}	1.03×10^{50}
55-Mn	1.59×10^{53}	2.22×10^{53}	2.08×10^{53}	2.71×10^{53}	5.15×10^{53}	6.18×10^{53}	8.56×10^{53}
54-Fe	8.73×10^{53}	1.49×10^{54}	1.68×10^{54}	1.7×10^{54}	3.96×10^{54}	4.9×10^{54}	1.11×10^{55}
56-Fe	8.38×10^{55}	8.41×10^{55}					
57-Fe	1.19×10^{54}	1.37×10^{54}	1.05×10^{54}	1.04×10^{54}	5.59×10^{53}	5.79×10^{53}	6×10^{53}
58-Fe	6.79×10^{46}	2.11×10^{47}	9.67×10^{47}	1.26×10^{48}	2.77×10^{48}	2.71×10^{47}	1.69×10^{49}
59-Co	2.11×10^{53}	1.58×10^{53}	1.93×10^{53}	1.8×10^{53}	1.88×10^{52}	2.96×10^{51}	2.24×10^{51}
58-Ni	4.61×10^{53}	4.96×10^{53}	4.59×10^{53}	4.53×10^{53}	3.51×10^{53}	4.58×10^{53}	6.88×10^{53}
60-Ni	2.54×10^{54}	1.94×10^{54}	1.88×10^{54}	1.61×10^{54}	1.77×10^{53}	4.31×10^{51}	5.25×10^{51}
61-Ni	4.32×10^{52}	3.76×10^{52}	2.54×10^{52}	2.22×10^{52}	6.91×10^{50}	7.23×10^{48}	1.58×10^{48}
62-Ni	2.32×10^{52}	1.81×10^{52}	1.62×10^{52}	1.43×10^{52}	4.65×10^{50}	1.96×10^{48}	6.42×10^{47}
64-Ni	4.59×10^{42}	1.19×10^{44}	1.31×10^{43}	7.31×10^{43}	3.92×10^{45}	3.9×10^{43}	9.23×10^{42}
63-Cu	5.86×10^{51}	4.24×10^{51}	4.7×10^{51}	4.12×10^{51}	1.47×10^{50}	2.84×10^{47}	2.47×10^{46}
65-Cu	2.56×10^{50}	2.9×10^{50}	1.95×10^{50}	1.7×10^{50}	9.33×10^{48}	1.23×10^{45}	1.56×10^{44}
64-Zn	1.5×10^{53}	1.46×10^{53}	1.14×10^{53}	9.93×10^{52}	3.04×10^{51}	3.62×10^{47}	5.22×10^{46}
66-Zn	8.19×10^{50}	1.28×10^{51}	6.05×10^{50}	5.08×10^{50}	1.9×10^{49}	4.23×10^{45}	6.16×10^{44}
67-Zn	1.94×10^{49}	2.79×10^{49}	1.56×10^{49}	1.26×10^{49}	2.59×10^{47}	7.56×10^{44}	1.01×10^{44}
68-Zn	3.52×10^{49}	3.88×10^{49}	4.82×10^{49}	4.11×10^{49}	9.64×10^{47}	1.56×10^{45}	3.14×10^{44}
70-Zn	8.31×10^{41}	4.3×10^{43}	7.89×10^{42}	3.01×10^{43}	4.76×10^{43}	2.23×10^{43}	5.33×10^{41}
69-Ga	9.35×10^{48}	6.73×10^{48}	7.31×10^{48}	5.91×10^{48}	1.05×10^{47}	6.06×10^{44}	5.1×10^{42}
71-Ga	1.02×10^{43}	1.34×10^{44}	2.2×10^{43}	1.1×10^{44}	2.68×10^{44}	2.8×10^{43}	1.63×10^{42}
140- χ	0	0	0	0	0	0	0
100- ρ	0	0	0	0	0	0	0

Table 2
Number of Nucleons of Each Isotope when the Metallicity Equals .001

$M_*(M_\odot)$	13	15	18	20	25	30	40
p	7.71×10^{57}	8.92×10^{57}	1.01×10^{58}	1.01×10^{58}	1.17×10^{58}	1.32×10^{58}	1.55×10^{58}
d	8.61×10^{42}	4.05×10^{45}	3.68×10^{42}	5.21×10^{41}	5.34×10^{41}	6.02×10^{41}	8.42×10^{43}
3-He	1.71×10^{53}	1.83×10^{53}	1.88×10^{53}	1.92×10^{53}	1.51×10^{53}	1.72×10^{53}	1.45×10^{53}
4-He	4.62×10^{57}	6.18×10^{57}	7.83×10^{57}	7.11×10^{57}	8.35×10^{57}	1.00×10^{58}	1.31×10^{58}
$H_{e_{nuc}}$	2.08×10^{56}	5.69×10^{56}	8.72×10^{56}	3.20×10^{56}	2.24×10^{56}	2.74×10^{56}	2.68×10^{56}
6-Li	2.84×10^{40}	1.33×10^{40}	1.06×10^{40}	2.87×10^{34}	2.81×10^{36}	3.29×10^{34}	2.74×10^{41}
7-Li	7.59×10^{47}	4.50×10^{44}	6.98×10^{44}	1.01×10^{47}	1.09×10^{45}	1.34×10^{45}	8.00×10^{45}
9-Be	2.79×10^{40}	1.09×10^{42}	1.12×10^{41}	1.71×10^{34}	2.46×10^{32}	0.00×10^{00}	4.86×10^{41}
10-B	1.38×10^{46}	7.20×10^{45}	7.87×10^{45}	2.84×10^{45}	9.10×10^{45}	2.69×10^{45}	2.41×10^{45}
11-B	6.12×10^{46}	3.21×10^{46}	3.52×10^{46}	1.23×10^{46}	4.10×10^{46}	1.21×10^{46}	8.40×10^{45}
12-C	1.28×10^{56}	1.02×10^{56}	1.55×10^{56}	1.53×10^{56}	2.58×10^{56}	1.45×10^{56}	8.83×10^{55}
13-C	2.00×10^{53}	6.44×10^{52}	8.62×10^{52}	2.35×10^{52}	1.18×10^{53}	9.82×10^{52}	3.38×10^{53}
14-N	1.09×10^{55}	4.29×10^{54}	5.35×10^{54}	1.55×10^{55}	1.10×10^{55}	7.41×10^{54}	1.04×10^{55}
15-N	9.07×10^{51}	1.03×10^{51}	1.10×10^{51}	1.64×10^{51}	8.67×10^{51}	4.54×10^{50}	2.92×10^{51}
16-O	6.04×10^{56}	3.52×10^{56}	5.05×10^{56}	2.61×10^{57}	4.58×10^{57}	6.38×10^{57}	1.00×10^{58}
17-O	8.34×10^{52}	3.07×10^{52}	2.90×10^{52}	2.61×10^{52}	3.34×10^{52}	5.83×10^{52}	3.43×10^{52}
18-O	2.17×10^{54}	4.38×10^{53}	3.67×10^{53}	9.69×10^{51}	8.44×10^{52}	3.22×10^{52}	3.15×10^{52}
19-F	3.68×10^{51}	2.37×10^{50}	3.98×10^{50}	3.35×10^{51}	7.33×10^{50}	2.86×10^{51}	5.35×10^{51}
20-Ne	7.91×10^{55}	2.28×10^{56}	2.12×10^{56}	7.51×10^{56}	1.46×10^{57}	1.74×10^{57}	3.44×10^{56}
21-Ne	2.22×10^{53}	8.08×10^{52}	1.05×10^{53}	1.64×10^{53}	6.10×10^{53}	7.32×10^{53}	1.33×10^{53}
22-Ne	1.59×10^{54}	3.28×10^{53}	5.69×10^{53}	1.40×10^{54}	1.76×10^{54}	1.87×10^{54}	1.05×10^{54}
23-Na	6.48×10^{53}	2.35×10^{54}	2.50×10^{54}	2.17×10^{54}	9.69×10^{54}	8.22×10^{54}	1.08×10^{54}
24-Mg	7.62×10^{55}	7.63×10^{55}	7.10×10^{55}	2.90×10^{56}	2.14×10^{56}	3.43×10^{56}	8.43×10^{56}
25-Mg	1.68×10^{54}	1.05×10^{54}	1.13×10^{54}	2.87×10^{54}	2.08×10^{54}	4.25×10^{54}	2.65×10^{54}
26-Mg	9.87×10^{53}	1.37×10^{54}	1.11×10^{54}	2.91×10^{54}	2.38×10^{54}	5.10×10^{54}	1.32×10^{54}
26-Al	1.21×10^{52}	2.19×10^{51}	3.73×10^{51}	4.28×10^{51}	3.33×10^{51}	9.17×10^{51}	5.99×10^{51}
27-Al	4.28×10^{54}	2.81×10^{54}	2.77×10^{54}	8.36×10^{54}	6.05×10^{54}	1.05×10^{55}	3.61×10^{55}
28-Si	1.08×10^{56}	5.14×10^{55}	1.83×10^{56}	1.53×10^{56}	1.44×10^{56}	1.98×10^{56}	1.06×10^{57}
29-Si	1.70×10^{54}	4.58×10^{53}	7.20×10^{53}	1.33×10^{54}	5.27×10^{53}	1.23×10^{54}	7.23×10^{54}
30-Si	2.22×10^{54}	5.09×10^{53}	6.40×10^{53}	9.29×10^{53}	3.29×10^{53}	8.49×10^{53}	1.21×10^{55}
31-P	6.36×10^{53}	9.73×10^{52}	2.24×10^{53}	2.36×10^{53}	1.28×10^{53}	2.44×10^{53}	4.17×10^{54}
32-S	4.43×10^{55}	1.96×10^{55}	9.44×10^{55}	6.73×10^{55}	6.60×10^{55}	9.34×10^{55}	3.94×10^{56}
33-S	2.35×10^{53}	5.70×10^{52}	3.61×10^{53}	1.19×10^{53}	9.73×10^{52}	1.66×10^{53}	1.00×10^{54}
34-S	1.10×10^{54}	2.86×10^{53}	7.63×10^{53}	3.71×10^{53}	2.14×10^{53}	4.41×10^{53}	2.54×10^{54}
36-S	8.97×10^{50}	1.86×10^{50}	3.83×10^{50}	4.85×10^{50}	7.82×10^{50}	1.08×10^{51}	6.66×10^{50}
35-Cl	9.77×10^{52}	9.70×10^{51}	9.77×10^{52}	2.79×10^{52}	2.52×10^{52}	4.01×10^{52}	4.22×10^{53}
37-Cl	1.72×10^{52}	3.15×10^{51}	4.95×10^{52}	1.22×10^{52}	1.55×10^{52}	2.30×10^{52}	7.56×10^{52}
36-Ar	6.82×10^{54}	2.95×10^{54}	1.46×10^{55}	1.21×10^{55}	1.11×10^{55}	1.62×10^{55}	5.46×10^{55}
38-Ar	3.21×10^{53}	2.71×10^{52}	4.93×10^{53}	1.28×10^{53}	9.88×10^{52}	1.95×10^{53}	1.00×10^{54}
40-Ar	2.11×10^{50}	5.87×10^{49}	1.23×10^{50}	6.50×10^{49}	1.18×10^{50}	1.41×10^{50}	8.18×10^{49}
39-K	3.01×10^{52}	4.97×10^{51}	6.82×10^{52}	1.66×10^{52}	1.82×10^{52}	2.84×10^{52}	1.33×10^{53}
40-K	3.19×10^{49}	2.34×10^{48}	4.70×10^{49}	9.07×10^{48}	1.19×10^{49}	1.14×10^{49}	2.85×10^{49}
41-K	2.89×10^{51}	3.75×10^{50}	1.31×10^{52}	2.48×10^{51}	2.66×10^{51}	4.77×10^{51}	1.82×10^{52}
40-Ca	5.67×10^{54}	2.07×10^{54}	9.65×10^{54}	1.10×10^{55}	9.51×10^{54}	1.40×10^{55}	4.38×10^{55}
42-Ca	7.93×10^{51}	4.85×10^{50}	1.62×10^{52}	3.34×10^{51}	2.98×10^{51}	5.56×10^{51}	2.74×10^{52}
43-Ca	4.97×10^{50}	4.01×10^{50}	2.93×10^{50}	2.29×10^{50}	3.47×10^{50}	4.25×10^{50}	3.37×10^{50}
44-Ca	2.97×10^{52}	2.48×10^{52}	2.24×10^{52}	5.85×10^{51}	9.53×10^{51}	7.71×10^{51}	1.32×10^{52}
46-Ca	7.97×10^{49}	1.69×10^{49}	3.05×10^{49}	4.01×10^{49}	3.62×10^{49}	8.49×10^{49}	1.46×10^{50}
48-Ca	3.78×10^{50}	1.16×10^{50}	1.46×10^{50}	1.50×10^{50}	1.88×10^{50}	2.23×10^{50}	2.60×10^{50}
45-Sc	3.02×10^{50}	6.08×10^{49}	4.25×10^{50}	2.59×10^{50}	3.88×10^{50}	5.05×10^{50}	1.19×10^{51}

46-Ti	4.77×10^{51}	1.49×10^{52}	6.12×10^{51}	1.63×10^{51}	1.57×10^{51}	2.58×10^{51}	1.20×10^{52}
47-Ti	3.05×10^{51}	1.53×10^{52}	1.80×10^{51}	5.15×10^{50}	4.02×10^{50}	5.39×10^{50}	7.61×10^{50}
48-Ti	1.16×10^{53}	6.22×10^{52}	1.20×10^{53}	1.64×10^{53}	1.40×10^{53}	2.00×10^{53}	3.03×10^{53}
49-Ti	4.61×10^{51}	2.32×10^{51}	4.95×10^{51}	8.12×10^{51}	6.80×10^{51}	1.01×10^{52}	1.68×10^{52}
50-Ti	7.57×10^{50}	1.94×10^{50}	2.23×10^{50}	6.05×10^{50}	1.02×10^{51}	1.37×10^{51}	1.39×10^{51}
50-V	1.32×10^{49}	1.34×10^{48}	2.17×10^{48}	1.02×10^{49}	1.57×10^{49}	2.47×10^{49}	1.11×10^{50}
51-V	1.07×10^{52}	1.94×10^{52}	9.06×10^{51}	9.86×10^{51}	9.01×10^{51}	1.19×10^{52}	2.32×10^{52}
50-Cr	2.52×10^{52}	1.59×10^{52}	3.58×10^{52}	2.84×10^{52}	3.29×10^{52}	4.20×10^{52}	1.62×10^{53}
52-Cr	1.44×10^{54}	3.63×10^{53}	1.82×10^{54}	2.66×10^{54}	2.61×10^{54}	3.50×10^{54}	4.72×10^{54}
53-Cr	8.90×10^{52}	3.38×10^{52}	1.09×10^{53}	1.64×10^{53}	1.33×10^{53}	2.12×10^{53}	3.07×10^{53}
54-Cr	2.24×10^{51}	5.75×10^{50}	7.14×10^{50}	1.69×10^{51}	2.61×10^{51}	3.28×10^{51}	3.40×10^{51}
55-Mn	2.72×10^{53}	9.59×10^{52}	3.37×10^{53}	4.55×10^{53}	3.58×10^{53}	6.00×10^{53}	9.41×10^{53}
54-Fe	1.83×10^{54}	8.47×10^{53}	2.47×10^{54}	2.84×10^{54}	2.69×10^{54}	3.96×10^{54}	1.25×10^{55}
56-Fe	8.70×10^{55}	8.48×10^{55}	8.52×10^{55}	8.49×10^{55}	8.52×10^{55}	8.53×10^{55}	8.56×10^{55}
57-Fe	1.69×10^{54}	2.10×10^{54}	1.52×10^{54}	8.64×10^{53}	6.35×10^{53}	6.98×10^{53}	6.89×10^{53}
58-Fe	6.80×10^{52}	1.57×10^{52}	1.86×10^{52}	5.98×10^{52}	9.32×10^{52}	1.11×10^{53}	1.22×10^{53}
59-Co	1.07×10^{53}	2.78×10^{53}	7.55×10^{52}	7.44×10^{52}	4.10×10^{52}	6.46×10^{52}	5.29×10^{52}
58-Ni	6.10×10^{53}	1.09×10^{54}	2.11×10^{54}	4.24×10^{53}	3.01×10^{53}	4.54×10^{53}	9.34×10^{53}
60-Ni	1.94×10^{54}	3.08×10^{54}	1.40×10^{54}	3.53×10^{53}	7.87×10^{52}	2.32×10^{53}	1.21×10^{53}
61-Ni	6.05×10^{52}	8.29×10^{52}	5.55×10^{52}	1.46×10^{52}	1.88×10^{52}	2.52×10^{52}	2.47×10^{52}
62-Ni	1.21×10^{53}	2.24×10^{53}	3.56×10^{53}	3.03×10^{52}	4.44×10^{52}	6.17×10^{52}	9.10×10^{52}
64-Ni	1.94×10^{52}	2.19×10^{51}	2.75×10^{51}	2.84×10^{52}	5.17×10^{52}	7.74×10^{52}	9.38×10^{52}
63-Cu	9.64×10^{51}	6.55×10^{51}	3.33×10^{51}	1.15×10^{52}	1.72×10^{52}	2.36×10^{52}	1.68×10^{52}
65-Cu	5.81×10^{51}	1.06×10^{51}	1.37×10^{51}	9.64×10^{51}	1.78×10^{52}	2.67×10^{52}	3.47×10^{52}
64-Zn	8.56×10^{52}	7.79×10^{52}	6.37×10^{52}	1.40×10^{52}	1.08×10^{52}	1.93×10^{52}	1.55×10^{52}
66-Zn	1.18×10^{52}	4.74×10^{51}	9.26×10^{51}	1.34×10^{52}	2.31×10^{52}	3.70×10^{52}	5.73×10^{52}
67-Zn	1.25×10^{51}	1.69×10^{50}	2.24×10^{50}	2.44×10^{51}	4.62×10^{51}	7.26×10^{51}	5.01×10^{51}
68-Zn	8.23×10^{51}	6.97×10^{50}	9.41×10^{50}	1.18×10^{52}	2.23×10^{52}	3.77×10^{52}	5.55×10^{52}
70-Zn	2.74×10^{50}	1.26×10^{49}	2.10×10^{49}	3.43×10^{49}	2.81×10^{49}	8.83×10^{49}	1.66×10^{50}
69-Ga	8.52×10^{50}	8.90×10^{49}	1.35×10^{50}	1.49×10^{51}	2.79×10^{51}	4.47×10^{51}	5.67×10^{51}
71-Ga	7.59×10^{50}	6.14×10^{49}	9.22×10^{49}	1.31×10^{51}	2.41×10^{51}	4.60×10^{51}	6.53×10^{51}
140- χ	4.50×10^{57}	5.70×10^{57}	7.16×10^{57}	7.14×10^{57}	8.83×10^{57}	1.09×10^{58}	1.54×10^{58}
100- ρ	1.56×10^{55}	1.80×10^{55}	2.16×10^{55}	2.40×10^{55}	2.99×10^{55}	3.59×10^{55}	4.79×10^{55}

Table 3
Number of Nucleons of Each Isotope of Each Star when the Metallicity Equals .004

$M_*(M_\odot)$	13	15	18	20	25	30	40
p	7.63×10^{57}	8.52×10^{57}	8.95×10^{57}	1.07×10^{58}	1.22×10^{58}	1.21×10^{58}	1.23×10^{58}
d	1.28×10^{43}	2.38×10^{43}	5.47×10^{43}	1.05×10^{44}	3.87×10^{41}	8.30×10^{43}	3.16×10^{41}
3-He	2.04×10^{53}	1.90×10^{53}	2.68×10^{53}	2.10×10^{53}	2.22×10^{53}	2.20×10^{53}	2.16×10^{53}
4-He	4.84×10^{57}	5.93×10^{57}	7.26×10^{57}	8.42×10^{57}	1.02×10^{58}	9.49×10^{57}	9.73×10^{57}
He_{nuc}	9.15×10^{56}	1.40×10^{57}	1.83×10^{57}	2.38×10^{57}	2.61×10^{57}	4.31×10^{56}	-2.3×10^{57}
6-Li	4.12×10^{40}	7.79×10^{40}	1.80×10^{41}	3.46×10^{41}	6.22×10^{34}	2.67×10^{41}	2.56×10^{37}
7-Li	3.77×10^{42}	8.62×10^{43}	6.04×10^{44}	1.87×10^{45}	1.22×10^{44}	9.59×10^{44}	5.64×10^{45}
9-Be	1.28×10^{41}	1.29×10^{41}	1.89×10^{41}	6.60×10^{41}	5.85×10^{33}	4.53×10^{41}	7.19×10^{35}
10-B	3.05×10^{46}	3.05×10^{46}	1.86×10^{47}	3.49×10^{46}	3.70×10^{46}	3.64×10^{46}	7.87×10^{45}
11-B	1.38×10^{47}	1.38×10^{47}	8.35×10^{47}	5.51×10^{49}	1.66×10^{47}	1.64×10^{47}	3.35×10^{46}
12-C	1.05×10^{56}	1.06×10^{56}	1.26×10^{56}	1.17×10^{56}	1.58×10^{56}	2.18×10^{56}	5.49×10^{56}
13-C	2.25×10^{53}	2.50×10^{53}	7.22×10^{55}	3.50×10^{53}	4.58×10^{53}	4.06×10^{53}	4.41×10^{53}
14-N	1.09×10^{55}	1.55×10^{55}	8.71×10^{55}	2.20×10^{55}	3.77×10^{55}	2.40×10^{55}	3.11×10^{55}
15-N	8.19×10^{51}	1.04×10^{52}	6.41×10^{55}	3.33×10^{52}	1.14×10^{53}	5.96×10^{51}	6.00×10^{51}
16-O	4.61×10^{56}	3.50×10^{56}	6.24×10^{56}	1.19×10^{57}	2.64×10^{57}	5.74×10^{57}	9.53×10^{57}
17-O	1.05×10^{53}	1.04×10^{53}	1.33×10^{54}	1.25×10^{53}	1.34×10^{53}	1.44×10^{53}	1.90×10^{53}
18-O	2.34×10^{54}	1.16×10^{54}	6.23×10^{55}	1.53×10^{54}	1.02×10^{54}	5.21×10^{52}	1.00×10^{54}
19-F	2.37×10^{51}	2.55×10^{51}	1.45×10^{52}	6.42×10^{51}	1.02×10^{53}	1.39×10^{52}	1.25×10^{51}
20-Ne	1.58×10^{56}	1.49×10^{56}	2.40×10^{56}	3.32×10^{56}	9.82×10^{56}	1.12×10^{57}	2.25×10^{57}
21-Ne	2.22×10^{53}	1.71×10^{53}	1.20×10^{54}	3.09×10^{53}	4.59×10^{53}	8.64×10^{53}	1.40×10^{54}
22-Ne	1.26×10^{54}	9.03×10^{53}	4.99×10^{54}	2.59×10^{54}	5.47×10^{54}	7.40×10^{54}	3.44×10^{54}
23-Na	1.80×10^{54}	9.81×10^{53}	7.94×10^{54}	4.87×10^{54}	7.49×10^{54}	1.69×10^{55}	3.13×10^{55}
24-Mg	5.25×10^{55}	8.94×10^{55}	8.30×10^{55}	1.16×10^{56}	2.79×10^{56}	2.61×10^{56}	4.54×10^{56}
25-Mg	1.65×10^{54}	2.34×10^{54}	9.81×10^{54}	2.64×10^{54}	7.23×10^{54}	8.49×10^{54}	1.44×10^{55}
26-Mg	1.49×10^{54}	2.31×10^{54}	7.71×10^{54}	2.25×10^{54}	8.04×10^{54}	8.47×10^{54}	1.59×10^{55}
26-Al	3.21×10^{51}	5.74×10^{51}	2.71×10^{52}	1.04×10^{52}	4.42×10^{51}	1.41×10^{52}	2.67×10^{52}
27-Al	2.65×10^{54}	3.96×10^{54}	7.53×10^{54}	6.14×10^{54}	1.34×10^{55}	2.02×10^{55}	3.64×10^{55}
28-Si	7.32×10^{55}	1.23×10^{56}	1.13×10^{56}	1.49×10^{56}	1.43×10^{56}	4.73×10^{56}	6.26×10^{56}
29-Si	6.48×10^{53}	1.34×10^{54}	3.23×10^{54}	1.52×10^{54}	2.31×10^{54}	4.04×10^{54}	5.45×10^{54}
30-Si	7.86×10^{53}	1.55×10^{54}	4.66×10^{54}	1.93×10^{54}	1.89×10^{54}	5.77×10^{54}	7.79×10^{54}
31-P	1.80×10^{53}	3.28×10^{53}	8.82×10^{53}	4.64×10^{53}	4.62×10^{53}	1.22×10^{54}	1.77×10^{54}
32-S	3.21×10^{55}	4.12×10^{55}	4.87×10^{55}	6.17×10^{55}	4.17×10^{55}	2.28×10^{56}	2.71×10^{56}
33-S	1.09×10^{53}	2.19×10^{53}	3.14×10^{53}	2.26×10^{53}	1.99×10^{53}	5.20×10^{53}	5.45×10^{53}
34-S	5.11×10^{53}	1.15×10^{54}	2.85×10^{54}	1.09×10^{54}	8.65×10^{53}	2.43×10^{54}	2.81×10^{54}
36-S	8.50×10^{50}	1.19×10^{51}	9.33×10^{51}	1.63×10^{51}	3.21×10^{51}	7.31×10^{51}	1.43×10^{52}
35-Cl	3.19×10^{52}	6.24×10^{52}	1.31×10^{53}	6.54×10^{52}	6.35×10^{52}	1.47×10^{53}	1.87×10^{53}
37-Cl	1.21×10^{52}	1.98×10^{52}	5.51×10^{52}	2.46×10^{52}	3.63×10^{52}	9.33×10^{52}	1.35×10^{53}
36-Ar	5.39×10^{54}	5.16×10^{54}	8.34×10^{54}	9.57×10^{54}	5.67×10^{54}	3.70×10^{55}	4.17×10^{55}
38-Ar	1.99×10^{53}	5.92×10^{53}	8.90×10^{53}	3.67×10^{53}	3.20×10^{53}	1.17×10^{54}	1.37×10^{54}
40-Ar	2.75×10^{50}	4.48×10^{50}	3.05×10^{51}	3.95×10^{50}	4.28×10^{50}	1.11×10^{51}	1.38×10^{51}
39-K	2.13×10^{52}	3.83×10^{52}	8.62×10^{52}	3.74×10^{52}	3.16×10^{52}	1.22×10^{53}	1.19×10^{53}
40-K	9.32×10^{48}	1.09×10^{49}	8.00×10^{49}	2.22×10^{49}	4.00×10^{49}	9.47×10^{49}	8.88×10^{49}
41-K	2.24×10^{51}	2.95×10^{51}	8.52×10^{51}	3.75×10^{51}	4.11×10^{51}	1.56×10^{52}	1.62×10^{52}
40-Ca	4.68×10^{54}	3.69×10^{54}	7.33×10^{54}	7.79×10^{54}	4.52×10^{54}	3.10×10^{55}	3.39×10^{55}
42-Ca	4.98×10^{51}	1.15×10^{52}	2.17×10^{52}	8.76×10^{51}	7.19×10^{51}	3.17×10^{52}	3.57×10^{52}
43-Ca	4.08×10^{50}	4.31×10^{50}	2.31×10^{51}	6.26×10^{50}	9.52×10^{50}	1.18×10^{51}	1.71×10^{51}
44-Ca	2.48×10^{52}	2.75×10^{52}	4.07×10^{52}	2.50×10^{52}	3.17×10^{52}	1.81×10^{52}	2.25×10^{52}
46-Ca	8.83×10^{49}	1.41×10^{50}	8.16×10^{50}	1.32×10^{50}	1.53×10^{50}	2.36×10^{50}	3.88×10^{50}
48-Ca	3.86×10^{50}	4.82×10^{50}	2.84×10^{51}	6.01×10^{50}	7.41×10^{50}	7.76×10^{50}	9.34×10^{50}
45-Sc	2.59×10^{50}	2.97×10^{50}	1.62×10^{51}	4.32×10^{50}	6.35×10^{50}	1.31×10^{51}	1.96×10^{51}

46-Ti	6.18×10^{51}	7.29×10^{51}	9.81×10^{51}	4.24×10^{51}	6.16×10^{51}	1.46×10^{52}	1.68×10^{52}
47-Ti	6.47×10^{51}	4.07×10^{51}	5.57×10^{51}	1.59×10^{51}	7.74×10^{51}	1.75×10^{51}	2.44×10^{51}
48-Ti	9.79×10^{52}	8.88×10^{52}	1.64×10^{53}	1.37×10^{53}	1.07×10^{53}	2.79×10^{53}	3.21×10^{53}
49-Ti	4.18×10^{51}	3.37×10^{51}	8.68×10^{51}	6.22×10^{51}	4.90×10^{51}	1.63×10^{52}	2.06×10^{52}
50-Ti	7.01×10^{50}	6.72×10^{50}	4.46×10^{51}	1.29×10^{51}	2.69×10^{51}	4.91×10^{51}	9.22×10^{51}
50-V	5.52×10^{48}	5.92×10^{48}	4.86×10^{49}	1.21×10^{49}	2.37×10^{49}	6.44×10^{49}	1.16×10^{50}
51-V	1.57×10^{52}	1.15×10^{52}	1.47×10^{52}	9.59×10^{51}	1.69×10^{52}	2.12×10^{52}	2.64×10^{52}
50-Cr	2.10×10^{52}	3.25×10^{52}	4.00×10^{52}	3.67×10^{52}	2.96×10^{52}	1.03×10^{53}	1.45×10^{53}
52-Cr	1.33×10^{54}	1.15×10^{54}	2.17×10^{54}	1.99×10^{54}	1.49×10^{54}	4.47×10^{54}	4.87×10^{54}
53-Cr	8.12×10^{52}	7.07×10^{52}	1.47×10^{53}	1.25×10^{53}	8.64×10^{52}	2.91×10^{53}	3.31×10^{53}
54-Cr	2.10×10^{51}	2.20×10^{51}	1.28×10^{52}	3.73×10^{51}	6.94×10^{51}	1.04×10^{52}	1.66×10^{52}
55-Mn	2.40×10^{53}	2.05×10^{53}	5.61×10^{53}	3.94×10^{53}	2.80×10^{53}	9.12×10^{53}	1.00×10^{54}
54-Fe	1.49×10^{54}	1.47×10^{54}	3.15×10^{54}	2.84×10^{54}	1.69×10^{54}	8.49×10^{54}	1.12×10^{55}
56-Fe	8.70×10^{55}	8.74×10^{55}	1.04×10^{56}	8.86×10^{55}	8.95×10^{55}	8.94×10^{55}	8.95×10^{55}
57-Fe	1.26×10^{54}	1.35×10^{54}	4.79×10^{54}	1.46×10^{54}	1.26×10^{54}	8.56×10^{53}	8.76×10^{53}
58-Fe	5.71×10^{52}	5.86×10^{52}	3.19×10^{53}	1.10×10^{53}	2.22×10^{53}	3.46×10^{53}	5.20×10^{53}
59-Co	2.35×10^{53}	1.57×10^{53}	3.22×10^{53}	7.44×10^{52}	2.60×10^{53}	1.53×10^{53}	2.29×10^{53}
58-Ni	6.16×10^{53}	5.56×10^{53}	2.69×10^{55}	5.91×10^{53}	6.52×10^{53}	8.55×10^{53}	9.91×10^{53}
60-Ni	2.16×10^{54}	2.00×10^{54}	1.64×10^{54}	1.55×10^{54}	2.16×10^{54}	3.15×10^{53}	4.55×10^{53}
61-Ni	5.09×10^{52}	5.98×10^{52}	3.19×10^{53}	6.79×10^{52}	7.29×10^{52}	6.65×10^{52}	1.17×10^{53}
62-Ni	4.25×10^{52}	2.87×10^{52}	3.69×10^{54}	1.09×10^{53}	1.31×10^{53}	2.10×10^{53}	3.61×10^{53}
64-Ni	1.31×10^{52}	4.34×10^{51}	8.00×10^{52}	3.34×10^{52}	1.18×10^{53}	2.34×10^{53}	5.09×10^{53}
63-Cu	1.26×10^{52}	6.43×10^{51}	4.34×10^{52}	1.62×10^{52}	5.11×10^{52}	6.26×10^{52}	1.25×10^{53}
65-Cu	4.56×10^{51}	1.81×10^{51}	2.54×10^{52}	1.22×10^{52}	3.80×10^{52}	8.31×10^{52}	1.74×10^{53}
64-Zn	1.37×10^{53}	1.39×10^{53}	2.77×10^{52}	7.23×10^{52}	1.55×10^{53}	3.57×10^{52}	6.95×10^{52}
66-Zn	8.05×10^{51}	5.58×10^{51}	1.03×10^{53}	2.05×10^{52}	5.49×10^{52}	1.27×10^{53}	2.61×10^{53}
67-Zn	9.45×10^{50}	3.84×10^{50}	6.92×10^{51}	2.69×10^{51}	1.03×10^{52}	2.18×10^{52}	4.92×10^{52}
68-Zn	4.22×10^{51}	1.82×10^{51}	3.43×10^{52}	1.40×10^{52}	5.25×10^{52}	1.44×10^{53}	3.16×10^{53}
70-Zn	1.34×10^{50}	1.07×10^{50}	1.27×10^{51}	1.11×10^{50}	1.99×10^{50}	5.49×10^{50}	6.97×10^{50}
69-Ga	6.06×10^{50}	2.08×10^{50}	3.45×10^{51}	1.86×10^{51}	6.70×10^{51}	1.92×10^{52}	4.04×10^{52}
71-Ga	3.65×10^{50}	2.46×10^{50}	3.46×10^{51}	1.40×10^{51}	5.65×10^{51}	1.59×10^{52}	3.50×10^{52}
140- χ	4.08×10^{57}	5.26×10^{57}	7.12×10^{57}	6.61×10^{57}	8.67×10^{57}	1.20×10^{58}	2.05×10^{58}
100- ρ	6.23×10^{55}	7.19×10^{55}	8.62×10^{55}	9.58×10^{55}	1.20×10^{56}	1.44×10^{56}	1.92×10^{56}

Table 4
Number of Nucleons of Each Isotope of Each Star when the Metallicity Equals .02

$M_*(M_\odot)$	13	15	18	20	25	30	40
p	7.37×10^{57}	8.13×10^{57}	9.02×10^{57}	9.50×10^{57}	1.01×10^{58}	1.05×10^{58}	4.25×10^{57}
d	9.99×10^{42}	1.22×10^{43}	4.98×10^{41}	1.44×10^{42}	1.18×10^{42}	1.29×10^{42}	9.23×10^{40}
3-He	2.35×10^{53}	2.61×10^{53}	2.75×10^{53}	2.85×10^{53}	2.65×10^{53}	2.54×10^{53}	6.05×10^{52}
4-He	5.15×10^{57}	6.29×10^{57}	7.32×10^{57}	8.10×10^{57}	8.67×10^{57}	1.00×10^{58}	5.64×10^{57}
He_{nuc}	1.23×10^{57}	1.76×10^{57}	1.89×10^{57}	2.06×10^{57}	1.13×10^{57}	9.58×10^{56}	-6.4×10^{57}
6-Li	1.58×10^{40}	3.80×10^{40}	3.33×10^{38}	1.31×10^{35}	1.14×10^{35}	7.07×10^{34}	4.16×10^{35}
7-Li	6.74×10^{46}	8.49×10^{44}	3.35×10^{44}	5.17×10^{45}	8.30×10^{44}	5.19×10^{44}	6.85×10^{44}
9-Be	5.52×10^{38}	1.86×10^{39}	9.06×10^{39}	5.65×10^{34}	2.67×10^{37}	5.89×10^{34}	8.42×10^{34}
10-B	1.34×10^{47}	1.63×10^{47}	1.70×10^{47}	1.76×10^{47}	1.81×10^{47}	1.84×10^{47}	8.34×10^{43}
11-B	5.13×10^{47}	7.21×10^{47}	7.68×10^{47}	7.83×10^{47}	8.11×10^{47}	8.29×10^{47}	3.86×10^{43}
12-C	1.28×10^{56}	7.80×10^{55}	1.63×10^{56}	2.93×10^{56}	1.82×10^{56}	2.99×10^{56}	7.14×10^{56}
13-C	1.20×10^{54}	1.38×10^{54}	1.65×10^{54}	1.74×10^{54}	7.98×10^{55}	2.30×10^{54}	5.16×10^{53}
14-N	5.75×10^{55}	7.37×10^{55}	7.92×10^{55}	8.61×10^{55}	1.01×10^{56}	1.22×10^{56}	6.96×10^{55}
15-N	4.90×10^{52}	7.15×10^{52}	1.83×10^{52}	2.68×10^{53}	5.55×10^{55}	7.85×10^{51}	6.85×10^{51}
16-O	2.61×10^{56}	1.94×10^{56}	9.22×10^{56}	1.26×10^{57}	2.81×10^{57}	3.86×10^{57}	8.78×10^{57}
17-O	1.04×10^{54}	9.73×10^{53}	1.05×10^{54}	1.14×10^{54}	1.61×10^{54}	2.02×10^{54}	1.16×10^{54}
18-O	4.19×10^{54}	3.04×10^{54}	1.40×10^{55}	6.25×10^{54}	1.01×10^{56}	7.40×10^{54}	1.47×10^{55}
19-F	1.70×10^{52}	1.96×10^{52}	5.35×10^{51}	7.25×10^{52}	1.43×10^{53}	9.35×10^{51}	6.30×10^{51}
20-Ne	4.16×10^{55}	4.06×10^{55}	1.78×10^{56}	4.72×10^{56}	1.02×10^{57}	1.12×10^{57}	2.65×10^{57}
21-Ne	2.69×10^{53}	1.56×10^{53}	2.42×10^{53}	2.17×10^{54}	1.90×10^{54}	3.56×10^{54}	5.95×10^{54}
22-Ne	5.41×10^{54}	2.06×10^{54}	7.94×10^{54}	1.08×10^{55}	2.01×10^{55}	2.23×10^{55}	1.31×10^{55}
23-Na	1.11×10^{54}	1.27×10^{54}	3.51×10^{54}	2.01×10^{55}	2.23×10^{55}	4.16×10^{55}	9.29×10^{55}
24-Mg	3.02×10^{55}	4.54×10^{55}	1.23×10^{56}	8.58×10^{55}	2.61×10^{56}	2.25×10^{56}	3.71×10^{56}
25-Mg	3.07×10^{54}	1.75×10^{54}	8.48×10^{54}	1.72×10^{55}	3.75×10^{55}	3.74×10^{55}	8.72×10^{55}
26-Mg	2.59×10^{54}	2.06×10^{54}	7.02×10^{54}	1.06×10^{55}	3.26×10^{55}	3.34×10^{55}	8.78×10^{55}
26-Al	2.55×10^{52}	9.14×10^{51}	4.42×10^{52}	1.80×10^{52}	1.04×10^{53}	4.67×10^{52}	7.95×10^{52}
27-Al	1.80×10^{54}	2.92×10^{54}	1.20×10^{55}	1.19×10^{55}	3.23×10^{55}	4.08×10^{55}	9.94×10^{55}
28-Si	8.96×10^{55}	1.00×10^{56}	1.21×10^{56}	7.57×10^{55}	1.53×10^{56}	2.87×10^{56}	2.89×10^{56}
29-Si	1.78×10^{54}	2.64×10^{54}	8.34×10^{54}	2.44×10^{54}	8.46×10^{54}	8.84×10^{54}	1.20×10^{55}
30-Si	1.86×10^{54}	3.29×10^{54}	8.17×10^{54}	2.92×10^{54}	7.41×10^{54}	1.27×10^{55}	1.17×10^{55}
31-P	4.49×10^{53}	8.46×10^{53}	2.08×10^{54}	7.88×10^{53}	1.80×10^{54}	3.07×10^{54}	4.22×10^{54}
32-S	4.47×10^{55}	4.16×10^{55}	4.42×10^{55}	3.37×10^{55}	5.98×10^{55}	1.29×10^{56}	1.31×10^{56}
33-S	2.40×10^{53}	2.91×10^{53}	4.20×10^{53}	2.71×10^{53}	3.89×10^{53}	5.76×10^{53}	5.76×10^{53}
34-S	1.96×10^{54}	1.83×10^{54}	2.62×10^{54}	2.04×10^{54}	2.71×10^{54}	4.50×10^{54}	4.10×10^{54}
36-S	6.43×10^{51}	3.04×10^{51}	1.44×10^{52}	1.10×10^{52}	2.90×10^{52}	6.10×10^{52}	1.13×10^{53}
35-Cl	1.38×10^{53}	1.64×10^{53}	2.10×10^{53}	1.50×10^{53}	1.94×10^{53}	2.79×10^{53}	3.31×10^{53}
37-Cl	3.63×10^{52}	2.98×10^{52}	6.77×10^{52}	1.01×10^{53}	2.04×10^{53}	3.15×10^{53}	6.76×10^{53}
36-Ar	7.53×10^{54}	5.87×10^{54}	6.56×10^{54}	5.58×10^{54}	9.49×10^{54}	2.17×10^{55}	2.17×10^{55}
38-Ar	8.22×10^{53}	7.80×10^{53}	9.38×10^{53}	8.07×10^{53}	1.08×10^{54}	1.96×10^{54}	1.98×10^{54}
40-Ar	1.07×10^{51}	1.26×10^{51}	1.56×10^{51}	1.69×10^{51}	3.21×10^{51}	8.88×10^{51}	6.79×10^{51}
39-K	6.01×10^{52}	8.38×10^{52}	9.19×10^{52}	8.85×10^{52}	1.06×10^{53}	1.55×10^{53}	1.37×10^{53}
40-K	1.53×10^{50}	7.70×10^{49}	1.65×10^{50}	1.11×10^{50}	2.40×10^{50}	3.52×10^{50}	4.85×10^{50}
41-K	5.61×10^{51}	7.01×10^{51}	9.27×10^{51}	1.08×10^{52}	1.66×10^{52}	2.36×10^{52}	5.41×10^{52}
40-Ca	5.89×10^{54}	4.80×10^{54}	5.44×10^{54}	4.48×10^{54}	7.85×10^{54}	1.88×10^{55}	1.87×10^{55}
42-Ca	1.66×10^{52}	2.10×10^{52}	2.48×10^{52}	2.08×10^{52}	2.96×10^{52}	4.97×10^{52}	5.37×10^{52}
43-Ca	1.63×10^{51}	1.80×10^{51}	2.54×10^{51}	3.02×10^{51}	4.10×10^{51}	3.56×10^{51}	5.91×10^{51}
44-Ca	4.20×10^{52}	4.25×10^{52}	6.53×10^{52}	6.94×10^{52}	6.12×10^{52}	4.84×10^{52}	5.59×10^{52}
46-Ca	2.54×10^{50}	3.99×10^{50}	9.38×10^{50}	7.37×10^{50}	1.41×10^{51}	1.41×10^{51}	3.43×10^{51}
48-Ca	1.89×10^{51}	2.23×10^{51}	3.27×10^{51}	2.81×10^{51}	3.27×10^{51}	1.70×10^{52}	2.91×10^{51}
45-Sc	8.73×10^{50}	1.11×10^{51}	1.51×10^{51}	1.56×10^{51}	3.35×10^{51}	3.08×10^{51}	7.37×10^{51}

46-Ti	7.20×10^{51}	1.03×10^{52}	1.14×10^{52}	1.02×10^{52}	1.35×10^{52}	2.23×10^{52}	2.53×10^{52}
47-Ti	5.28×10^{51}	4.12×10^{51}	6.40×10^{51}	7.85×10^{51}	6.70×10^{51}	1.06×10^{52}	8.08×10^{51}
48-Ti	9.74×10^{52}	1.28×10^{53}	1.58×10^{53}	1.38×10^{53}	1.83×10^{53}	3.03×10^{53}	2.92×10^{53}
49-Ti	5.68×10^{51}	6.07×10^{51}	7.32×10^{51}	7.63×10^{51}	1.32×10^{52}	2.30×10^{52}	2.90×10^{52}
50-Ti	2.79×10^{51}	2.89×10^{51}	4.68×10^{51}	6.97×10^{51}	1.47×10^{52}	1.19×10^{52}	4.56×10^{52}
50-V	2.43×10^{49}	3.19×10^{49}	7.91×10^{49}	4.66×10^{49}	1.15×10^{50}	2.98×10^{50}	2.24×10^{50}
51-V	1.41×10^{52}	1.19×10^{52}	1.37×10^{52}	1.59×10^{52}	1.72×10^{52}	2.99×10^{52}	2.68×10^{52}
50-Cr	2.67×10^{52}	4.73×10^{52}	4.41×10^{52}	3.71×10^{52}	6.25×10^{52}	9.23×10^{52}	1.10×10^{53}
52-Cr	7.76×10^{53}	1.52×10^{54}	1.53×10^{54}	1.28×10^{54}	2.44×10^{54}	4.50×10^{54}	4.53×10^{54}
53-Cr	7.47×10^{52}	1.11×10^{53}	1.15×10^{53}	9.92×10^{52}	1.69×10^{53}	3.28×10^{53}	2.98×10^{53}
54-Cr	7.85×10^{51}	8.14×10^{51}	1.82×10^{52}	1.99×10^{52}	3.32×10^{52}	6.13×10^{52}	6.78×10^{52}
55-Mn	3.37×10^{53}	4.55×10^{53}	4.85×10^{53}	4.31×10^{53}	6.59×10^{53}	1.25×10^{54}	9.92×10^{53}
54-Fe	2.30×10^{54}	2.95×10^{54}	2.98×10^{54}	2.66×10^{54}	4.60×10^{54}	8.23×10^{54}	7.69×10^{54}
56-Fe	9.97×10^{55}	1.02×10^{56}	1.04×10^{56}	1.06×10^{56}	1.08×10^{56}	1.10×10^{56}	9.68×10^{55}
57-Fe	2.66×10^{54}	2.38×10^{54}	3.20×10^{54}	2.80×10^{54}	2.24×10^{54}	3.38×10^{54}	1.17×10^{54}
58-Fe	1.45×10^{53}	1.32×10^{53}	7.02×10^{53}	5.94×10^{53}	1.00×10^{54}	2.86×10^{54}	1.77×10^{54}
59-Co	1.69×10^{53}	1.08×10^{53}	2.18×10^{53}	3.50×10^{53}	4.66×10^{53}	6.46×10^{53}	8.31×10^{53}
58-Ni	2.67×10^{54}	1.37×10^{54}	3.23×10^{54}	2.20×10^{54}	1.87×10^{54}	1.86×10^{54}	1.06×10^{54}
60-Ni	2.55×10^{54}	2.24×10^{54}	2.54×10^{54}	2.98×10^{54}	2.17×10^{54}	7.33×10^{53}	1.44×10^{54}
61-Ni	9.83×10^{52}	1.49×10^{53}	1.25×10^{53}	1.78×10^{53}	2.59×10^{53}	1.32×10^{53}	4.68×10^{53}
62-Ni	2.72×10^{53}	1.96×10^{53}	5.56×10^{53}	4.62×10^{53}	7.92×10^{53}	2.66×10^{53}	1.40×10^{54}
64-Ni	4.01×10^{52}	2.06×10^{52}	3.58×10^{52}	2.24×10^{53}	7.38×10^{53}	8.52×10^{52}	2.66×10^{54}
63-Cu	2.19×10^{52}	1.56×10^{52}	2.28×10^{52}	1.53×10^{53}	3.52×10^{53}	1.03×10^{53}	8.20×10^{53}
65-Cu	1.23×10^{52}	8.60×10^{51}	9.13×10^{51}	5.27×10^{52}	1.75×10^{53}	1.56×10^{52}	7.77×10^{53}
64-Zn	1.16×10^{53}	8.11×10^{52}	6.88×10^{52}	1.44×10^{53}	6.43×10^{52}	2.24×10^{52}	2.01×10^{53}
66-Zn	2.08×10^{52}	2.13×10^{52}	2.60×10^{52}	7.50×10^{52}	2.86×10^{53}	1.84×10^{52}	1.28×10^{54}
67-Zn	3.45×10^{51}	2.13×10^{51}	2.43×10^{51}	1.55×10^{52}	6.30×10^{52}	3.26×10^{51}	2.97×10^{53}
68-Zn	1.58×10^{52}	8.97×10^{51}	1.40×10^{52}	7.22×10^{52}	3.76×10^{53}	1.52×10^{52}	1.86×10^{54}
70-Zn	2.19×10^{51}	6.70×10^{50}	6.14×10^{50}	1.94×10^{51}	1.01×10^{52}	4.42×10^{50}	3.17×10^{52}
69-Ga	2.00×10^{51}	1.01×10^{51}	1.09×10^{51}	7.98×10^{51}	3.28×10^{52}	1.65×10^{51}	2.10×10^{53}
71-Ga	1.77×10^{51}	9.53×10^{50}	1.27×10^{51}	6.16×10^{51}	3.34×10^{52}	1.32×10^{51}	1.58×10^{53}
140- χ	4.25×10^{57}	5.55×10^{57}	6.92×10^{57}	8.01×10^{57}	1.16×10^{58}	1.55×10^{58}	3.38×10^{58}
100- ρ	3.11×10^{56}	3.59×10^{56}	4.31×10^{56}	4.79×10^{56}	5.99×10^{56}	7.19×10^{56}	9.58×10^{56}

Table 5
Initial Total Number of Nucleons of Each Star

$M_*(M_\odot)$	13	15	18	20	25	30	40
β_i	1.56×10^{58}	1.80×10^{58}	2.16×10^{58}	2.40×10^{58}	2.99×10^{58}	3.59×10^{58}	4.79×10^{58}

Table 6
 ϵ_{sum} of Each Star when only Metallicity Varies, Subscripts Next to ϵ_{sum} Indicate the Metallicity of Stars in the Row

$M_*(M_\odot)$	13	15	18	20	25	30	40
ϵ_{sum0}	2.53×10^{58}	3.95×10^{58}	6.14×10^{58}	8.53×10^{58}	1.09×10^{59}	1.53×10^{59}	2.56×10^{59}
$\epsilon_{sum.001}$	3.61×10^{58}	3.38×10^{58}	5.98×10^{58}	1.26×10^{59}	2.20×10^{59}	3.26×10^{59}	5.99×10^{59}
$\epsilon_{sum.004}$	4.23×10^{58}	1.24×10^{59}	2.72×10^{59}	1.24×10^{59}	2.39×10^{59}	5.57×10^{59}	1.41×10^{60}
$\epsilon_{sum.02}$	3.95×10^{58}	1.33×10^{59}	2.11×10^{59}	2.86×10^{59}	6.06×10^{59}	9.61×10^{59}	3.17×10^{60}

Table 7

Progress of Nucleosynthesis within Each Star when the Metallicity Varies, Subscripts Next to P Indicate the Metallicity of Stars in the Row

$M_*(M_\odot)$	13	15	18	20	25	30	40
P_0	1.63×10^{00}	2.20×10^{00}	2.85×10^{00}	3.56×10^{00}	3.64×10^{00}	4.26×10^{00}	5.34×10^{00}
$P_{.001}$	2.32×10^{00}	1.88×10^{00}	2.77×10^{00}	5.28×10^{00}	7.34×10^{00}	9.08×10^{00}	1.25×10^{01}
$P_{.004}$	2.72×10^{00}	6.88×10^{00}	1.26×10^{01}	5.17×10^{00}	7.98×10^{00}	1.55×10^{01}	2.94×10^{01}
$P_{.02}$	2.54×10^{00}	7.40×10^{00}	9.78×10^{00}	1.19×10^{01}	2.02×10^{01}	2.67×10^{01}	6.61×10^{02}

Table 8

Average Rate of Nucleosynthesis of Each Star When Only the Metallicity Varies, Subscripts Next to η Indicate the Metallicity of Stars in the Row

$M_*(M_\odot)$	13	15	18	20	25	30	40
η_0	4.28×10^{60}	8.88×10^{60}	1.99×10^{61}	3.41×10^{61}	6.81×10^{61}	1.38×10^{62}	4.09×10^{62}
$\eta_{.001}$	6.10×10^{60}	7.61×10^{60}	1.94×10^{61}	5.06×10^{61}	1.37×10^{62}	2.94×10^{62}	9.58×10^{62}
$\eta_{.004}$	7.15×10^{60}	2.78×10^{61}	8.83×10^{61}	4.95×10^{61}	1.49×10^{62}	5.01×10^{62}	2.25×10^{63}
$\eta_{.02}$	6.68×10^{60}	2.99×10^{61}	6.83×10^{61}	1.14×10^{62}	3.79×10^{62}	8.65×10^{62}	5.07×10^{63}

Table 9

Coefficients and Powers for the Trend Line of Figure 1

Metallicity	Coefficient	Power
0	2.28×10^{-1}	0.86
0.001	5.28×10^{-2}	1.50
0.004	3.71×10^{-2}	1.80
0.02	4.48×10^{-3}	2.60

Table 10

Coefficients and Powers for the Trend Line of Figures 2

Metallicity	Coefficient	Power
0	3.74×10^{56}	3.77
0.001	1.93×10^{56}	4.18
0.004	6.94×10^{54}	5.31
0.02	1.48×10^{54}	5.95

Table 11
Number of Nucleons of Each Isotope when the Metallicity Equals 0

$M_*(M_\odot)$	20	25	30	40
E (erg^{51})	10	10	20	30
p	1.05×10^{58}	1.27×10^{58}	1.40×10^{58}	1.68×10^{58}
d	1.04×10^{41}	2.47×10^{41}	1.31×10^{43}	1.99×10^{43}
3-He	5.70×10^{52}	2.53×10^{53}	2.47×10^{53}	3.07×10^{52}
4-He	7.14×10^{57}	9.62×10^{57}	1.14×10^{58}	1.41×10^{58}
He_{nuc}	3.28×10^{56}	6.66×10^{56}	7.54×10^{56}	6.08×10^{56}
6-Li	1.83×10^{35}	3.86×10^{37}	4.19×10^{40}	6.46×10^{40}
7-Li	3.34×10^{47}	6.80×10^{48}	2.83×10^{49}	4.10×10^{46}
9-Be	5.79×10^{37}	4.42×10^{40}	3.70×10^{39}	1.08×10^{40}
10-B	2.34×10^{38}	8.92×10^{43}	1.26×10^{43}	1.13×10^{43}
11-B	1.31×10^{42}	1.53×10^{45}	1.14×10^{44}	1.13×10^{45}
12-C	2.28×10^{56}	3.20×10^{56}	3.78×10^{56}	4.46×10^{56}
13-C	1.41×10^{49}	8.31×10^{49}	7.57×10^{49}	9.80×10^{49}
14-N	6.49×10^{52}	7.14×10^{53}	5.01×10^{52}	4.06×10^{51}
15-N	3.53×10^{49}	2.10×10^{50}	2.64×10^{50}	7.83×10^{50}
16-O	2.43×10^{57}	2.85×10^{57}	4.70×10^{57}	7.57×10^{57}
17-O	8.54×10^{49}	1.78×10^{51}	4.56×10^{49}	1.47×10^{49}
18-O	2.79×10^{49}	4.64×10^{50}	6.02×10^{50}	3.51×10^{50}
19-F	2.54×10^{48}	2.00×10^{48}	9.44×10^{48}	1.40×10^{50}
20-Ne	8.97×10^{56}	3.41×10^{56}	6.23×10^{56}	3.16×10^{56}
21-Ne	4.29×10^{52}	1.46×10^{52}	4.20×10^{52}	1.69×10^{52}
22-Ne	6.60×10^{52}	1.03×10^{52}	4.22×10^{52}	1.99×10^{52}
23-Na	2.77×10^{54}	5.29×10^{53}	8.82×10^{53}	3.93×10^{53}
24-Mg	1.98×10^{56}	1.83×10^{56}	2.60×10^{56}	4.04×10^{56}
25-Mg	1.28×10^{53}	5.47×10^{52}	1.74×10^{53}	7.13×10^{53}
26-Mg	2.50×10^{53}	4.66×10^{52}	9.58×10^{52}	8.26×10^{52}
26-Al	1.22×10^{51}	1.53×10^{51}	3.50×10^{51}	4.55×10^{52}
27-Al	1.80×10^{54}	1.07×10^{54}	1.86×10^{54}	9.01×10^{54}
28-Si	1.23×10^{56}	2.77×10^{56}	2.96×10^{56}	8.62×10^{56}
29-Si	3.53×10^{53}	6.44×10^{53}	1.06×10^{54}	4.46×10^{54}
30-Si	1.35×10^{53}	7.61×10^{52}	1.76×10^{53}	3.38×10^{54}
31-P	9.19×10^{52}	7.08×10^{52}	1.39×10^{53}	1.21×10^{54}
32-S	5.11×10^{55}	1.10×10^{56}	1.02×10^{56}	3.10×10^{56}
33-S	1.72×10^{53}	2.77×10^{53}	3.62×10^{53}	1.01×10^{54}
34-S	2.20×10^{53}	1.51×10^{53}	3.23×10^{53}	2.49×10^{54}
36-S	9.98×10^{47}	6.92×10^{46}	1.69×10^{48}	6.04×10^{49}
35-Cl	4.73×10^{52}	3.87×10^{52}	5.37×10^{52}	2.16×10^{53}
37-Cl	2.25×10^{52}	3.46×10^{52}	2.86×10^{52}	9.52×10^{52}
36-Ar	8.14×10^{54}	1.63×10^{55}	1.38×10^{55}	4.25×10^{55}
38-Ar	1.52×10^{53}	2.04×10^{53}	1.09×10^{53}	9.38×10^{53}
40-Ar	4.54×10^{46}	1.39×10^{46}	2.24×10^{46}	3.21×10^{47}
39-K	2.77×10^{52}	4.50×10^{52}	2.46×10^{52}	1.57×10^{53}
40-K	5.27×10^{48}	1.68×10^{48}	3.02×10^{48}	1.41×10^{49}
41-K	4.46×10^{51}	7.76×10^{51}	4.38×10^{51}	2.55×10^{52}
40-Ca	5.71×10^{54}	1.22×10^{55}	9.85×10^{54}	3.43×10^{55}
42-Ca	4.08×10^{51}	6.17×10^{51}	1.94×10^{51}	2.36×10^{52}
43-Ca	3.11×10^{50}	8.68×10^{49}	2.05×10^{50}	1.66×10^{50}
44-Ca	1.51×10^{53}	8.43×10^{52}	2.18×10^{53}	2.10×10^{53}
46-Ca	1.38×10^{46}	1.76×10^{46}	1.11×10^{46}	4.42×10^{46}
48-Ca	4.48×10^{42}	1.40×10^{46}	9.77×10^{44}	1.52×10^{46}
45-Sc	2.22×10^{50}	2.64×10^{50}	8.32×10^{49}	7.52×10^{50}

46-Ti	7.83×10^{51}	6.25×10^{51}	7.46×10^{51}	1.33×10^{52}
47-Ti	1.16×10^{52}	1.13×10^{52}	2.49×10^{52}	3.10×10^{52}
48-Ti	1.88×10^{53}	1.62×10^{53}	3.37×10^{53}	4.11×10^{53}
49-Ti	3.29×10^{51}	4.34×10^{51}	6.83×10^{51}	8.29×10^{51}
50-Ti	9.15×10^{44}	7.33×10^{45}	2.98×10^{45}	4.04×10^{46}
50-V	3.14×10^{46}	3.34×10^{46}	1.08×10^{46}	1.44×10^{47}
51-V	2.90×10^{52}	2.23×10^{52}	4.44×10^{52}	4.17×10^{52}
50-Cr	2.01×10^{52}	3.07×10^{52}	2.28×10^{52}	4.93×10^{52}
52-Cr	7.88×10^{53}	1.45×10^{54}	1.81×10^{54}	3.23×10^{54}
53-Cr	3.99×10^{52}	8.67×10^{52}	1.08×10^{53}	1.57×10^{53}
54-Cr	3.13×10^{48}	6.85×10^{48}	1.15×10^{47}	4.22×10^{48}
55-Mn	9.85×10^{52}	2.42×10^{53}	2.96×10^{53}	4.41×10^{53}
54-Fe	8.60×10^{53}	2.14×10^{54}	2.08×10^{54}	3.95×10^{54}
56-Fe	9.87×10^{55}	1.15×10^{56}	1.90×10^{56}	3.07×10^{56}
57-Fe	2.13×10^{54}	1.95×10^{54}	3.71×10^{54}	5.08×10^{54}
58-Fe	1.53×10^{48}	3.11×10^{48}	1.10×10^{47}	3.96×10^{48}
59-Co	4.42×10^{53}	2.85×10^{53}	6.22×10^{53}	6.22×10^{53}
58-Ni	1.05×10^{54}	8.05×10^{53}	1.52×10^{54}	1.71×10^{54}
60-Ni	3.58×10^{54}	3.35×10^{54}	6.58×10^{54}	1.00×10^{55}
61-Ni	7.53×10^{52}	5.20×10^{52}	1.03×10^{53}	1.18×10^{53}
62-Ni	5.02×10^{52}	3.43×10^{52}	6.88×10^{52}	8.07×10^{52}
64-Ni	1.14×10^{44}	1.87×10^{46}	4.05×10^{45}	2.95×10^{46}
63-Cu	1.41×10^{52}	9.81×10^{51}	2.05×10^{52}	2.47×10^{52}
65-Cu	8.67×10^{50}	7.19×10^{50}	1.65×10^{51}	2.23×10^{51}
64-Zn	4.55×10^{53}	3.16×10^{53}	6.98×10^{53}	8.24×10^{53}
66-Zn	6.06×10^{51}	3.10×10^{51}	8.44×10^{51}	8.26×10^{51}
67-Zn	2.34×10^{50}	7.27×10^{49}	2.29×10^{50}	1.41×10^{50}
68-Zn	1.07×10^{50}	1.45×10^{50}	3.22×10^{50}	5.82×10^{50}
70-Zn	9.95×10^{43}	2.34×10^{45}	1.02×10^{45}	2.34×10^{46}
69-Ga	2.12×10^{49}	2.53×10^{49}	4.89×10^{49}	1.07×10^{50}
71-Ga	1.84×10^{45}	2.60×10^{46}	4.54×10^{45}	1.88×10^{47}
140- χ	0	0	0	0
100- ρ	0	0	0	0

Table 12
Number of Nucleons of Each Isotope when the Metallicity Equals .001

$M_*(M_\odot)$	20	25	30	40
E (erg^{51})	10	10	20	30
p	1.01×10^{58}	1.17×10^{58}	1.32×10^{58}	1.55×10^{58}
d	4.91×10^{41}	5.34×10^{41}	1.83×10^{44}	3.19×10^{42}
3-He	1.92×10^{53}	1.51×10^{53}	1.72×10^{53}	1.45×10^{53}
4-He	7.14×10^{57}	8.38×10^{57}	1.01×10^{58}	1.29×10^{58}
He_{nuc}	3.28×10^{56}	2.35×10^{56}	2.89×10^{56}	2.33×10^{56}
6-Li	1.12×10^{36}	5.68×10^{36}	6.08×10^{41}	9.16×10^{39}
7-Li	1.01×10^{47}	1.09×10^{45}	1.34×10^{45}	2.29×10^{45}
9-Be	2.06×10^{36}	3.04×10^{32}	3.10×10^{41}	1.62×10^{39}
10-B	2.84×10^{45}	9.10×10^{45}	2.69×10^{45}	2.42×10^{45}
11-B	1.26×10^{46}	4.10×10^{46}	1.21×10^{46}	1.00×10^{46}
12-C	1.49×10^{56}	2.32×10^{56}	1.26×10^{56}	6.08×10^{55}
13-C	2.35×10^{52}	1.18×10^{53}	9.82×10^{52}	3.38×10^{53}
14-N	1.55×10^{55}	1.10×10^{55}	7.41×10^{54}	1.02×10^{55}
15-N	1.64×10^{51}	8.67×10^{51}	1.09×10^{51}	3.80×10^{51}
16-O	2.40×10^{57}	4.43×10^{57}	5.92×10^{57}	7.69×10^{57}
17-O	2.61×10^{52}	3.34×10^{52}	5.83×10^{52}	3.39×10^{52}
18-O	9.70×10^{51}	8.44×10^{52}	2.38×10^{52}	2.11×10^{53}
19-F	3.35×10^{51}	7.27×10^{50}	2.44×10^{51}	1.98×10^{51}
20-Ne	5.46×10^{56}	1.26×10^{57}	1.25×10^{57}	2.19×10^{56}
21-Ne	1.16×10^{53}	5.07×10^{53}	5.31×10^{53}	2.59×10^{52}
22-Ne	1.40×10^{54}	1.72×10^{54}	1.51×10^{54}	1.50×10^{53}
23-Na	1.55×10^{54}	8.10×10^{54}	5.61×10^{54}	7.23×10^{53}
24-Mg	2.75×10^{56}	2.31×10^{56}	3.73×10^{56}	6.23×10^{56}
25-Mg	2.08×10^{54}	1.82×10^{54}	3.34×10^{54}	1.96×10^{54}
26-Mg	2.10×10^{54}	2.10×10^{54}	3.83×10^{54}	1.08×10^{54}
26-Al	5.63×10^{51}	4.40×10^{51}	1.14×10^{52}	2.42×10^{52}
27-Al	7.57×10^{54}	6.19×10^{54}	1.04×10^{55}	2.35×10^{55}
28-Si	1.37×10^{56}	1.34×10^{56}	2.81×10^{56}	8.55×10^{56}
29-Si	1.53×10^{54}	9.34×10^{53}	2.02×10^{54}	7.45×10^{54}
30-Si	1.28×10^{54}	5.82×10^{53}	1.49×10^{54}	9.58×10^{54}
31-P	3.25×10^{53}	2.20×10^{53}	4.73×10^{53}	3.20×10^{54}
32-S	4.35×10^{55}	5.09×10^{55}	1.11×10^{56}	3.35×10^{56}
33-S	2.16×10^{53}	2.55×10^{53}	4.92×10^{53}	1.44×10^{54}
34-S	6.12×10^{53}	4.98×10^{53}	1.22×10^{54}	4.48×10^{54}
36-S	3.96×10^{50}	6.79×10^{50}	1.13×10^{51}	1.19×10^{51}
35-Cl	4.55×10^{52}	6.42×10^{52}	1.21×10^{53}	4.25×10^{53}
37-Cl	1.65×10^{52}	2.30×10^{52}	4.49×10^{52}	1.06×10^{53}
36-Ar	6.65×10^{54}	8.22×10^{54}	1.68×10^{55}	4.40×10^{55}
38-Ar	1.71×10^{53}	1.41×10^{53}	4.32×10^{53}	1.49×10^{54}
40-Ar	5.41×10^{49}	1.04×10^{50}	3.04×10^{50}	4.66×10^{50}
39-K	2.46×10^{52}	2.11×10^{52}	6.50×10^{52}	1.93×10^{53}
40-K	8.23×10^{48}	1.32×10^{49}	1.47×10^{49}	3.73×10^{49}
41-K	3.16×10^{51}	2.69×10^{51}	8.48×10^{51}	2.47×10^{52}
40-Ca	5.38×10^{54}	6.54×10^{54}	1.32×10^{55}	3.51×10^{55}
42-Ca	4.43×10^{51}	2.61×10^{51}	9.71×10^{51}	3.71×10^{52}
43-Ca	4.53×10^{50}	5.91×10^{50}	7.73×10^{50}	4.89×10^{50}
44-Ca	1.56×10^{53}	1.59×10^{53}	2.92×10^{53}	1.88×10^{53}
46-Ca	2.95×10^{49}	3.19×10^{49}	1.32×10^{50}	2.28×10^{50}
48-Ca	1.43×10^{50}	1.81×10^{50}	2.17×10^{50}	2.56×10^{50}
45-Sc	2.55×10^{50}	3.81×10^{50}	6.65×10^{50}	1.25×10^{51}

46-Ti	4.54×10^{51}	1.61×10^{52}	1.56×10^{52}	1.82×10^{52}
47-Ti	5.79×10^{51}	3.35×10^{52}	3.92×10^{52}	2.31×10^{52}
48-Ti	1.98×10^{53}	2.16×10^{53}	3.89×10^{53}	3.99×10^{53}
49-Ti	3.23×10^{51}	3.28×10^{51}	6.48×10^{51}	1.05×10^{52}
50-Ti	4.90×10^{50}	8.98×10^{50}	1.08×10^{51}	9.14×10^{50}
50-V	8.59×10^{48}	1.47×10^{49}	2.06×10^{49}	6.05×10^{49}
51-V	1.43×10^{52}	6.53×10^{52}	5.67×10^{52}	3.29×10^{52}
50-Cr	1.49×10^{52}	2.41×10^{52}	3.21×10^{52}	6.58×10^{52}
52-Cr	8.85×10^{53}	1.08×10^{54}	1.83×10^{54}	3.56×10^{54}
53-Cr	4.76×10^{52}	4.56×10^{52}	8.52×10^{52}	1.95×10^{53}
54-Cr	1.38×10^{51}	2.34×10^{51}	2.73×10^{51}	2.36×10^{51}
55-Mn	1.31×10^{53}	1.34×10^{53}	2.35×10^{53}	5.58×10^{53}
54-Fe	1.01×10^{54}	1.41×10^{54}	2.32×10^{54}	4.86×10^{54}
56-Fe	9.65×10^{55}	1.80×10^{56}	2.40×10^{56}	3.10×10^{56}
57-Fe	2.46×10^{54}	3.34×10^{54}	4.59×10^{54}	5.04×10^{54}
58-Fe	4.71×10^{52}	8.19×10^{52}	9.31×10^{52}	7.91×10^{52}
59-Co	1.86×10^{53}	7.91×10^{53}	9.41×10^{53}	5.38×10^{53}
58-Ni	6.78×10^{53}	1.32×10^{54}	2.02×10^{54}	1.66×10^{54}
60-Ni	3.29×10^{54}	7.39×10^{54}	8.41×10^{54}	9.50×10^{54}
61-Ni	1.01×10^{53}	1.37×10^{53}	1.57×10^{53}	1.57×10^{53}
62-Ni	6.58×10^{52}	1.23×10^{53}	1.39×10^{53}	1.40×10^{53}
64-Ni	2.18×10^{52}	4.53×10^{52}	5.83×10^{52}	5.37×10^{52}
63-Cu	1.75×10^{52}	4.02×10^{52}	4.65×10^{52}	3.14×10^{52}
65-Cu	9.33×10^{51}	1.74×10^{52}	2.49×10^{52}	2.60×10^{52}
64-Zn	3.99×10^{53}	6.26×10^{53}	9.40×10^{53}	7.80×10^{53}
66-Zn	2.06×10^{52}	2.95×10^{52}	4.91×10^{52}	5.86×10^{52}
67-Zn	2.01×10^{51}	4.19×10^{51}	5.80×10^{51}	3.05×10^{51}
68-Zn	9.40×10^{51}	2.00×10^{52}	2.98×10^{52}	3.46×10^{52}
70-Zn	2.90×10^{49}	2.84×10^{49}	1.29×10^{50}	2.28×10^{50}
69-Ga	1.45×10^{51}	2.58×10^{51}	4.60×10^{51}	4.98×10^{51}
71-Ga	1.02×10^{51}	2.16×10^{51}	3.62×10^{51}	4.07×10^{51}
140- χ	3.79×10^{56}	7.27×10^{56}	1.58×10^{57}	2.76×10^{57}
100- ρ	2.40×10^{55}	2.99×10^{55}	3.59×10^{55}	4.79×10^{55}

Table 13
Number of Nucleons Present when the Metallicity Equals .004

$M_*(M_\odot)$	20	25	30	40
$E(\text{erg}^{51})$	10	10	20	30
p	1.07×10^{58}	1.22×10^{58}	1.21×10^{58}	1.23×10^{58}
d	2.20×10^{44}	2.41×10^{44}	3.46×10^{44}	4.65×10^{43}
3-He	2.10×10^{53}	2.22×10^{53}	2.20×10^{53}	2.16×10^{53}
4-He	8.42×10^{57}	1.02×10^{58}	9.50×10^{57}	9.73×10^{57}
He_{nuc}	8.38×10^{56}	8.91×10^{56}	1.17×10^{56}	-4.77×10^{56}
6-Li	7.33×10^{41}	7.97×10^{41}	1.15×10^{42}	1.53×10^{41}
7-Li	5.16×10^{44}	1.22×10^{44}	9.59×10^{44}	5.53×10^{45}
9-Be	7.51×10^{41}	4.71×10^{41}	2.25×10^{41}	1.14×10^{40}
10-B	3.49×10^{46}	3.70×10^{46}	3.64×10^{46}	7.87×10^{45}
11-B	3.34×10^{48}	1.66×10^{47}	1.64×10^{47}	3.39×10^{46}
12-C	9.97×10^{55}	1.53×10^{56}	1.63×10^{56}	4.47×10^{56}
13-C	3.49×10^{53}	4.59×10^{53}	4.06×10^{53}	4.41×10^{53}
14-N	2.20×10^{55}	3.77×10^{55}	2.40×10^{55}	3.02×10^{55}
15-N	3.28×10^{52}	1.13×10^{53}	6.70×10^{51}	1.62×10^{52}
16-O	9.44×10^{56}	2.48×10^{57}	4.58×10^{57}	8.14×10^{57}
17-O	1.23×10^{53}	1.34×10^{53}	1.44×10^{53}	1.88×10^{53}
18-O	8.00×10^{53}	9.34×10^{53}	5.25×10^{52}	7.80×10^{53}
19-F	5.83×10^{51}	1.02×10^{53}	6.67×10^{51}	1.02×10^{52}
20-Ne	1.70×10^{56}	7.61×10^{56}	5.89×10^{56}	1.38×10^{57}
21-Ne	3.74×10^{53}	4.28×10^{53}	4.95×10^{53}	1.03×10^{54}
22-Ne	1.70×10^{54}	5.44×10^{54}	3.59×10^{54}	9.57×10^{53}
23-Na	2.46×10^{54}	5.61×10^{54}	7.86×10^{54}	1.58×10^{55}
24-Mg	9.70×10^{55}	2.72×10^{56}	2.29×10^{56}	4.80×10^{56}
25-Mg	1.96×10^{54}	5.71×10^{54}	5.92×10^{54}	1.16×10^{55}
26-Mg	2.02×10^{54}	6.30×10^{54}	6.73×10^{54}	1.21×10^{55}
26-Al	7.11×10^{51}	8.91×10^{51}	1.86×10^{52}	3.68×10^{52}
27-Al	4.36×10^{54}	1.25×10^{55}	1.41×10^{55}	2.74×10^{55}
28-Si	1.25×10^{56}	1.46×10^{56}	4.26×10^{56}	6.88×10^{56}
29-Si	2.13×10^{54}	2.72×10^{54}	5.82×10^{54}	7.94×10^{54}
30-Si	2.38×10^{54}	2.78×10^{54}	5.77×10^{54}	8.83×10^{54}
31-P	5.61×10^{53}	6.34×10^{53}	1.62×10^{54}	2.40×10^{54}
32-S	3.95×10^{55}	4.82×10^{55}	1.84×10^{56}	2.75×10^{56}
33-S	3.51×10^{53}	3.65×10^{53}	1.26×10^{54}	1.82×10^{54}
34-S	1.66×10^{54}	1.50×10^{54}	5.74×10^{54}	8.65×10^{54}
36-S	6.17×10^{51}	2.77×10^{51}	1.05×10^{52}	1.47×10^{52}
35-Cl	8.94×10^{52}	9.71×10^{52}	3.47×10^{53}	4.98×10^{53}
37-Cl	2.86×10^{52}	4.08×10^{52}	1.27×10^{53}	1.89×10^{53}
36-Ar	5.27×10^{54}	7.21×10^{54}	2.73×10^{55}	4.07×10^{55}
38-Ar	5.13×10^{53}	4.53×10^{53}	2.13×10^{54}	2.97×10^{54}
40-Ar	1.75×10^{51}	4.56×10^{50}	3.44×10^{51}	2.31×10^{51}
39-K	5.17×10^{52}	4.97×10^{52}	2.06×10^{53}	2.58×10^{53}
40-K	2.69×10^{49}	3.94×10^{49}	1.02×10^{50}	1.29×10^{50}
41-K	5.25×10^{51}	5.58×10^{51}	2.28×10^{52}	2.78×10^{52}
40-Ca	3.67×10^{54}	5.62×10^{54}	2.00×10^{55}	3.05×10^{55}
42-Ca	1.31×10^{52}	1.10×10^{52}	5.32×10^{52}	6.96×10^{52}
43-Ca	1.31×10^{51}	1.14×10^{51}	1.34×10^{51}	2.61×10^{51}
44-Ca	3.43×10^{52}	1.27×10^{53}	1.34×10^{53}	2.71×10^{53}
46-Ca	2.81×10^{50}	1.71×10^{50}	8.31×10^{50}	5.13×10^{50}
48-Ca	1.28×10^{51}	7.22×10^{50}	1.17×10^{51}	1.63×10^{51}
45-Sc	7.28×10^{50}	7.33×10^{50}	1.82×10^{51}	2.14×10^{51}

46-Ti	5.41×10^{51}	9.43×10^{51}	2.38×10^{52}	3.05×10^{52}
47-Ti	1.88×10^{51}	1.05×10^{52}	1.46×10^{52}	1.49×10^{52}
48-Ti	5.86×10^{52}	1.90×10^{53}	2.75×10^{53}	5.15×10^{53}
49-Ti	1.78×10^{51}	5.34×10^{51}	7.77×10^{51}	1.39×10^{52}
50-Ti	9.93×10^{50}	2.35×10^{51}	3.04×10^{51}	5.81×10^{51}
50-V	1.22×10^{49}	2.42×10^{49}	4.91×10^{49}	9.08×10^{49}
51-V	3.80×10^{51}	2.71×10^{52}	2.61×10^{52}	3.28×10^{52}
50-Cr	1.78×10^{52}	2.46×10^{52}	6.82×10^{52}	9.62×10^{52}
52-Cr	3.22×10^{53}	1.02×10^{54}	2.05×10^{54}	3.93×10^{54}
53-Cr	2.56×10^{52}	6.42×10^{52}	1.27×10^{53}	2.38×10^{53}
54-Cr	2.80×10^{51}	6.17×10^{51}	6.90×10^{51}	1.11×10^{52}
55-Mn	1.08×10^{53}	2.00×10^{53}	3.90×10^{53}	6.96×10^{53}
54-Fe	9.77×10^{53}	1.40×10^{54}	3.59×10^{54}	5.95×10^{54}
56-Fe	3.73×10^{55}	9.97×10^{55}	1.83×10^{56}	3.27×10^{56}
57-Fe	1.19×10^{54}	2.31×10^{54}	3.96×10^{54}	7.50×10^{54}
58-Fe	6.56×10^{52}	1.94×10^{53}	2.12×10^{53}	3.40×10^{53}
59-Co	5.87×10^{52}	4.40×10^{53}	3.96×10^{53}	5.35×10^{53}
58-Ni	3.59×10^{53}	1.10×10^{54}	1.13×10^{54}	1.81×10^{54}
60-Ni	1.21×10^{54}	3.56×10^{54}	5.89×10^{54}	9.92×10^{54}
61-Ni	1.80×10^{53}	1.11×10^{53}	3.51×10^{53}	4.31×10^{53}
62-Ni	1.47×10^{53}	2.06×10^{53}	3.33×10^{53}	7.44×10^{53}
64-Ni	1.99×10^{52}	9.67×10^{52}	1.32×10^{53}	3.19×10^{53}
63-Cu	1.06×10^{52}	5.07×10^{52}	5.71×10^{52}	1.09×10^{53}
65-Cu	9.01×10^{51}	3.40×10^{52}	5.82×10^{52}	1.34×10^{53}
64-Zn	4.35×10^{52}	3.82×10^{53}	4.26×10^{53}	7.00×10^{53}
66-Zn	2.52×10^{52}	5.81×10^{52}	1.29×10^{53}	2.55×10^{53}
67-Zn	1.74×10^{51}	8.53×10^{51}	1.37×10^{52}	3.37×10^{52}
68-Zn	9.41×10^{51}	4.43×10^{52}	9.04×10^{52}	2.20×10^{53}
70-Zn	2.86×10^{50}	2.36×10^{50}	1.59×10^{51}	3.57×10^{51}
69-Ga	1.63×10^{51}	6.46×10^{51}	1.78×10^{52}	4.11×10^{52}
71-Ga	1.32×10^{51}	4.73×10^{51}	1.12×10^{52}	2.59×10^{52}
140- χ	9.39×10^{56}	1.44×10^{57}	5.22×10^{57}	1.12×10^{58}
100- ρ	9.58×10^{55}	1.20×10^{56}	1.44×10^{56}	1.92×10^{56}

Table 14
Number of Nucleons Present when the Metallicity Equals .02

$M_*(M_\odot)$	20	25	30	40
$E(\text{erg}^{51})$	10	10	20	30
p	9.50×10^{57}	1.01×10^{58}	1.05×10^{58}	4.25×10^{57}
d	2.96×10^{44}	2.36×10^{44}	8.68×10^{44}	1.71×10^{45}
3-He	2.85×10^{53}	2.65×10^{53}	2.54×10^{53}	6.05×10^{52}
4-He	8.10×10^{57}	8.68×10^{57}	1.00×10^{58}	5.73×10^{57}
He_{nuc}	6.96×10^{56}	3.30×10^{56}	2.71×10^{56}	-7.59×10^{56}
6-Li	9.85×10^{41}	7.86×10^{41}	2.89×10^{42}	5.69×10^{42}
7-Li	4.28×10^{45}	6.34×10^{44}	1.87×10^{43}	6.85×10^{44}
9-Be	1.45×10^{41}	2.22×10^{41}	8.36×10^{41}	2.91×10^{42}
10-B	1.76×10^{47}	1.81×10^{47}	1.86×10^{47}	8.91×10^{43}
11-B	7.93×10^{47}	8.13×10^{47}	8.34×10^{47}	4.55×10^{44}
12-C	2.50×10^{56}	1.72×10^{56}	2.14×10^{56}	5.87×10^{56}
13-C	1.74×10^{54}	7.97×10^{55}	2.30×10^{54}	5.16×10^{53}
14-N	8.61×10^{55}	1.01×10^{56}	1.22×10^{56}	6.96×10^{55}
15-N	3.03×10^{53}	5.55×10^{55}	1.84×10^{52}	5.10×10^{52}
16-O	1.17×10^{57}	2.61×10^{57}	3.28×10^{57}	8.44×10^{57}
17-O	1.14×10^{54}	1.61×10^{54}	2.01×10^{54}	1.16×10^{54}
18-O	4.77×10^{54}	1.00×10^{56}	3.34×10^{54}	1.25×10^{55}
19-F	8.29×10^{52}	1.41×10^{53}	1.12×10^{52}	1.18×10^{52}
20-Ne	3.50×10^{56}	7.75×10^{56}	6.48×10^{56}	2.08×10^{57}
21-Ne	2.37×10^{54}	2.04×10^{54}	3.08×10^{54}	6.22×10^{54}
22-Ne	1.06×10^{55}	1.99×10^{55}	1.35×10^{55}	1.28×10^{55}
23-Na	1.44×10^{55}	1.69×10^{55}	2.17×10^{55}	6.90×10^{55}
24-Mg	8.24×10^{55}	2.49×10^{56}	2.01×10^{56}	3.94×10^{56}
25-Mg	1.34×10^{55}	2.90×10^{55}	2.61×10^{55}	6.97×10^{55}
26-Mg	8.98×10^{54}	2.53×10^{55}	2.83×10^{55}	7.10×10^{55}
26-Al	2.17×10^{52}	7.46×10^{52}	5.80×10^{52}	1.16×10^{53}
27-Al	1.03×10^{55}	2.80×10^{55}	2.84×10^{55}	8.62×10^{55}
28-Si	1.13×10^{56}	1.49×10^{56}	3.20×10^{56}	3.93×10^{56}
29-Si	3.53×10^{54}	9.94×10^{54}	1.29×10^{55}	2.04×10^{55}
30-Si	4.18×10^{54}	1.32×10^{55}	1.80×10^{55}	2.36×10^{55}
31-P	1.17×10^{54}	2.38×10^{54}	4.37×10^{54}	6.50×10^{54}
32-S	5.69×10^{55}	5.21×10^{55}	1.29×10^{56}	1.68×10^{56}
33-S	6.32×10^{53}	7.27×10^{53}	1.70×10^{54}	2.07×10^{54}
34-S	4.52×10^{54}	5.22×10^{54}	1.68×10^{55}	2.02×10^{55}
36-S	1.56×10^{52}	2.67×10^{52}	7.07×10^{52}	1.01×10^{53}
35-Cl	3.21×10^{53}	1.89×10^{53}	7.25×10^{53}	9.86×10^{53}
37-Cl	1.16×10^{53}	1.68×10^{53}	2.79×10^{53}	6.24×10^{53}
36-Ar	8.80×10^{54}	7.94×10^{54}	1.69×10^{55}	2.37×10^{55}
38-Ar	1.46×10^{54}	6.95×10^{53}	5.40×10^{54}	6.16×10^{54}
40-Ar	3.82×10^{51}	3.95×10^{51}	1.63×10^{52}	9.63×10^{51}
39-K	1.64×10^{53}	8.12×10^{52}	3.09×10^{53}	3.07×10^{53}
40-K	2.14×10^{50}	2.69×10^{50}	6.10×10^{50}	1.11×10^{51}
41-K	1.64×10^{52}	1.33×10^{52}	3.17×10^{52}	5.57×10^{52}
40-Ca	5.98×10^{54}	6.79×10^{54}	1.11×10^{55}	1.70×10^{55}
42-Ca	4.23×10^{52}	1.61×10^{52}	1.34×10^{53}	1.49×10^{53}
43-Ca	3.40×10^{51}	4.28×10^{51}	7.31×10^{51}	9.06×10^{51}
44-Ca	6.13×10^{52}	1.19×10^{53}	1.53×10^{53}	4.95×10^{53}
46-Ca	1.09×10^{51}	1.59×10^{51}	2.86×10^{51}	4.44×10^{51}
48-Ca	3.53×10^{51}	3.32×10^{51}	1.47×10^{52}	3.22×10^{51}
45-Sc	2.19×10^{51}	3.25×10^{51}	5.32×10^{51}	8.16×10^{51}

46-Ti	1.99×10^{52}	8.77×10^{51}	5.47×10^{52}	6.73×10^{52}
47-Ti	6.83×10^{51}	9.69×10^{51}	1.53×10^{52}	4.78×10^{52}
48-Ti	8.83×10^{52}	1.99×10^{53}	2.72×10^{53}	7.10×10^{53}
49-Ti	5.28×10^{51}	9.87×10^{51}	1.40×10^{52}	2.20×10^{52}
50-Ti	6.24×10^{51}	1.27×10^{52}	1.02×10^{52}	3.96×10^{52}
50-V	7.11×10^{49}	1.68×10^{50}	4.41×10^{50}	4.42×10^{50}
51-V	1.31×10^{52}	1.86×10^{52}	2.97×10^{52}	7.88×10^{52}
50-Cr	8.47×10^{52}	2.42×10^{52}	1.18×10^{53}	1.45×10^{53}
52-Cr	4.92×10^{53}	1.11×10^{54}	1.74×10^{54}	2.96×10^{54}
53-Cr	6.64×10^{52}	9.01×10^{52}	1.61×10^{53}	1.72×10^{53}
54-Cr	1.77×10^{52}	2.90×10^{52}	4.46×10^{52}	5.98×10^{52}
55-Mn	3.81×10^{53}	4.23×10^{53}	7.01×10^{53}	5.92×10^{53}
54-Fe	4.54×10^{54}	2.54×10^{54}	4.83×10^{54}	7.05×10^{54}
56-Fe	4.28×10^{55}	1.06×10^{56}	1.25×10^{56}	3.32×10^{56}
57-Fe	1.46×10^{54}	3.39×10^{54}	4.92×10^{54}	1.07×10^{55}
58-Fe	5.08×10^{53}	8.82×10^{53}	2.11×10^{54}	1.63×10^{54}
59-Co	2.91×10^{53}	5.05×10^{53}	7.91×10^{53}	1.70×10^{54}
58-Ni	1.82×10^{54}	2.54×10^{54}	4.04×10^{54}	8.55×10^{54}
60-Ni	1.44×10^{54}	3.76×10^{54}	3.99×10^{54}	1.34×10^{55}
61-Ni	2.91×10^{53}	3.56×10^{53}	1.09×10^{54}	1.02×10^{54}
62-Ni	4.42×10^{53}	1.06×10^{54}	9.99×10^{53}	3.56×10^{54}
64-Ni	1.92×10^{53}	6.11×10^{53}	8.35×10^{52}	2.34×10^{54}
63-Cu	1.18×10^{53}	2.78×10^{53}	7.35×10^{52}	7.01×10^{53}
65-Cu	4.97×10^{52}	1.61×10^{53}	2.42×10^{52}	6.83×10^{53}
64-Zn	6.31×10^{52}	1.62×10^{53}	9.97×10^{52}	7.64×10^{53}
66-Zn	8.54×10^{52}	2.81×10^{53}	8.86×10^{52}	1.22×10^{54}
67-Zn	1.40×10^{52}	5.25×10^{52}	3.61×10^{51}	2.77×10^{53}
68-Zn	6.38×10^{52}	3.29×10^{53}	1.43×10^{52}	1.71×10^{54}
70-Zn	2.93×10^{51}	1.02×10^{52}	7.05×10^{50}	6.73×10^{52}
69-Ga	8.17×10^{51}	3.22×10^{52}	1.52×10^{51}	1.93×10^{53}
71-Ga	5.93×10^{51}	2.86×10^{52}	2.71×10^{51}	1.55×10^{53}
140- χ	2.00×10^{57}	4.11×10^{57}	6.57×10^{57}	2.18×10^{58}
100- ρ	4.79×10^{56}	5.99×10^{56}	7.19×10^{56}	9.58×10^{56}

Table 15

Initial Total Number of Nucleons of Each Star when Explosion Energies Vary

$M_*(M_\odot)$	20	25	30	40
E (erg^{51})	10	10	20	30
β_i	2.40×10^{58}	2.99×10^{58}	3.59×10^{58}	4.79×10^{58}

Table 16

ϵ_{sum} of Each Star when Explosion Energy Varies, Subscripts Next to ϵ_{sum} Indicate the Metallicity of Stars in the Row

$M_*(M_\odot)$	20	25	30	40
E (erg^{51})	10	10	20	30
ϵ_{sum0}	7.75×10^{58}	8.28×10^{58}	1.26×10^{59}	2.01×10^{59}
$\epsilon_{sum.001}$	5.44×10^{58}	1.03×10^{59}	2.22×10^{59}	3.87×10^{59}
$\epsilon_{sum.004}$	1.35×10^{59}	2.05×10^{59}	7.31×10^{59}	1.57×10^{60}
$\epsilon_{sum.02}$	2.78×10^{59}	6.05×10^{59}	9.51×10^{59}	3.20×10^{60}

Table 17

Progress of Nucleosynthesis in Stars when Metallicity and Explosion Energy Varies, Subscripts Next to P Indicate the Metallicity of Stars in the Row

$M_*(M_\odot)$	20	25	30	40
$E (erg^{51})$	10	10	20	30
P_0	3.24	2.77	3.50	4.20
$P_{.001}$	2.27	3.43	6.18	8.07
$P_{.004}$	5.63	6.83	20.35	32.80
$P_{.02}$	11.603	20.188	26.478	66.693

Table 18

Average Rate of Nucleosynthesis in Stars when Metallicity and Explosion Energy Varies, Subscripts Next to η Indicate the Metallicity of Stars in the Row

$M_*(M_\odot)$	20	25	30	40
$E (erg^{51})$	10	10	20	30
η_0	3.10×10^{61}	5.18×10^{61}	1.13×10^{62}	3.22×10^{62}
$\eta_{.001}$	2.17×10^{61}	6.42×10^{61}	2.00×10^{62}	6.19×10^{62}
$\eta_{.004}$	5.39×10^{61}	1.28×10^{62}	6.58×10^{62}	2.51×10^{63}
$\eta_{.02}$	1.11×10^{62}	3.78×10^{62}	8.56×10^{62}	5.11×10^{63}

Table 19

Coefficients and Powers for the Trend Line of Figure 3 when Explosion Energies Vary

Metallicity	Coefficient	Power
0	6.42×10^{-1}	0.50
0.001	1.88×10^{-2}	1.65
0.004	3.37×10^{-3}	2.50
0.02	2.61×10^{-3}	2.75

Table 20

Coefficients and Powers for the Trend Line of Figure 4 when Explosion Energies Vary

Metallicity	Coefficient	Power
0	4.11×10^{56}	3.68
0.001	8.67×10^{55}	4.28
0.004	1.86×10^{55}	5.08
0.02	1.17×10^{54}	6.02

Table 21

Flow of Nucleosynthesis in Stars when only Metallicity, Subscripts Next to ϕ Indicate the Metallicity of Stars in the Row

$M_*(M_\odot)$	13	15	18	20	25	30	40
ϕ_0	1.59×10^{57}	2.30×10^{57}	3.62×10^{57}	4.91×10^{57}	6.54×10^{57}	9.32×10^{57}	1.43×10^{58}
$\phi_{.001}$	1.33×10^{57}	1.39×10^{57}	2.12×10^{57}	4.5×10^{57}	7.3×10^{57}	9.89×10^{57}	1.5×10^{58}
$\phi_{.004}$	1.74×10^{57}	2.65×10^{57}	4.6×10^{57}	4.28×10^{57}	7.14×10^{57}	1.1×10^{58}	1.97×10^{58}
$\phi_{.02}$	1.70×10^{57}	2.67×10^{57}	4.2×10^{57}	5.41×10^{57}	9.1×10^{57}	1.25×10^{58}	2.86×10^{58}

Table 22

Flow of Nucleosynthesis in Stars when Metallicity and Explosion Energy Varies, Subscripts Next to ϕ Indicate the Metallicity of Stars in the Row

$M_*(M_\odot)$	20	25	30	40
$E (erg^{51})$	10	10	20	30
ϕ_0	4.08×10^{57}	4.59×10^{57}	6.91×10^{57}	1.03×10^{58}
$\phi_{.001}$	4.09×10^{57}	7.07×10^{57}	9.66×10^{57}	1.26×10^{58}
$\phi_{.004}$	2.95×10^{57}	5.81×10^{57}	1.13×10^{58}	2.19×10^{58}
$\phi_{.02}$	4.17×10^{57}	8.11×10^{57}	1.10×10^{58}	3.23×10^{58}

Table 23
Coefficients and Powers for the Trend Line of Figure 5

Metallicity	Coefficient	Power
0	2.64×10^{55}	1.71
0.001	1.29×10^{55}	1.92
0.004	9.80×10^{54}	2.06
0.02	2.71×10^{54}	2.51

Table 24
Coefficients and Powers for the Trend Line of Figure 6 when Explosion Energies Vary

Metallicity	Coefficient	Power
0	4.46×10^{55}	1.47
0.001	8.04×10^{55}	1.38
0.004	1.22×10^{54}	2.66
0.02	1.98×10^{53}	3.25

Table 25
AlphaK of Each Star when the Metallicity Varies, Subscripts Next to P Indicate the Metallicity of Stars in the Row

$M_*(M_\odot)$	13	15	18	20	25	30	40
α_0	1.64×10^{82}	2.73×10^{82}	5.17×10^{82}	7.80×10^{82}	1.30×10^{83}	2.22×10^{83}	4.53×10^{83}
$\alpha_{.001}$	1.64×10^{82}	2.73×10^{82}	5.17×10^{82}	7.80×10^{82}	1.30×10^{83}	2.22×10^{83}	4.53×10^{83}
$\alpha_{.004}$	1.64×10^{82}	2.73×10^{82}	5.17×10^{82}	7.80×10^{82}	1.30×10^{83}	2.22×10^{83}	4.53×10^{83}
$\alpha_{.02}$	1.76×10^{82}	3.18×10^{82}	6.00×10^{82}	8.59×10^{82}	1.81×10^{83}	2.98×10^{83}	9.09×10^{83}

Table 26
AlphaK of Each Star when the Metallicity and Explosion Energy Varies, Subscripts Next to P Indicate the Metallicity of Stars in the Row

$M_*(M_\odot)$	20	25	30	40
α_0	6.48×10^{82}	9.11×10^{82}	1.65×10^{83}	3.28×10^{83}
$\alpha_{.001}$	6.49×10^{82}	1.40×10^{83}	2.30×10^{83}	3.99×10^{83}
$\alpha_{.004}$	4.68×10^{82}	1.15×10^{83}	2.68×10^{83}	6.95×10^{83}
$\alpha_{.02}$	6.62×10^{82}	1.61×10^{83}	2.62×10^{83}	1.03×10^{84}

Table 27
Coefficients and Powers for the Trend Line of Figure 7

Metallicity	Coefficient	Power
0	2.75×10^{79}	2.63
0.001	1.93×10^{79}	2.74
0.004	7.54×10^{78}	3.07
0.02	1.58×10^{78}	3.60

Table 28
Coefficients and Powers for the Trend Line of Figure 8 when Explosion Energies Vary

Metallicity	Coefficient	Power
0	3.27×10^{79}	2.50
0.001	9.68×10^{79}	2.26
0.004	1.27×10^{78}	3.58
0.02	9.82×10^{76}	4.38